Sedimentary Geology 339 (2016) 218–233

Contents lists available at ScienceDirect

Sedimentary Geology

journal homepage: www.elsevier.com/locate/sedgeo

Muddy and dolomitic rip-up clasts in Triassic fluvial sandstones: Origin and impact on potential reservoir properties (Argana Basin, Morocco)

Saturnina Henares [a,*], Jose Arribas [b], Giuseppe Cultrone [c], Cesar Viseras [a]

[a] Departamento de Estratigrafía y Paleontología, Facultad de Ciencias, Universidad de Granada, 18071, Granada, Spain
[b] Departamento de Petrología y Geoquímica, Universidad Complutense de Madrid, IGEO-CSIC, 28040, Madrid, Spain
[c] Departamento de Mineralogía y Petrología, Facultad de Ciencias, Universidad de Granada, 18071, Granada, Spain

ARTICLE INFO

Article history:
Received 21 December 2015
Received in revised form 22 March 2016
Accepted 23 March 2016
Available online 1 April 2016

Editor: Dr. B. Jones

Keywords:
Triassic
Fluvial sandstones
Reservoir
Rip-up clasts
Dolomite
Diagenesis

ABSTRACT

The significance of rip-up clasts as sandstone framework grains is frequently neglected in the literature being considered as accessory components in bulk sandstone composition. However, this study highlights the great value of muddy and dolomitic rip-up clast occurrence as: (a) information source about low preservation potential from floodplain deposits and (b) key element controlling host sandstone diagenetic evolution and thus ultimate reservoir quality. High-resolution petrographic analysis on Triassic fluvial sandstones from Argana Basin (T6 and T7/T8 units) highlights the significance of different types of rip-up clasts as intrabasinal framework components of continental sediments from arid climates. On the basis of their composition and ductility, three main types are distinguished: (a) muddy rip-up clasts, (b) dolomitic muddy rip-up clasts and (c) dolomite crystalline rip-up clasts. Spatial distribution of different types is strongly facies-related according to grain size. Origin of rip-up clasts is related to erosion of coeval phreatic dolocretes, in different development stages, and associated muddy floodplain sediments. Cloudy cores with abundant inclusions and clear outer rims of dolomite crystals suggest a first replacive and a subsequent displacive growth, respectively. Dolomite crystals are almost stoichiometric. This composition is very similar to that of early sandstone dolomite cement, supporting phreatic dolocretes as dolomite origin in both situations. Sandstone diagenesis is dominated by mechanical compaction and dolomite cementation. A direct correlation exists between: (1) muddy rip-up clast abundance and early reduction of primary porosity by compaction with irreversible loss of intergranular volume (IGV); and (2) occurrence of dolomitic rip-up clasts and dolomite cement nucleation in host sandstone, occluding adjacent pores but preserving IGV. Both processes affect reservoir quality by generation of vertical and 3D fluid flow baffles and barriers that compartmentalize the reservoir. These findings may provide quantitative useful data for the better understanding of reservoir quality in analogous hydrocarbon-bearing basins such as the Bay of Fundy, Nova Scotia (Canada).

1. Introduction

Calcretes and dolocretes have been widely recognized in ancient fluvial sediments deposited under relative arid climates and saline/evaporate conditions (Goudie, 1983; Wright and Tucker, 1991; Milnes, 1992; Kraus, 1999). They may form as vadose (pedogenic) or phreatic (groundwater) mineral precipitates (Arakel, 1986; Wright, 1994; Colson and Cojan, 1996; Chen et al., 2002). Genesis of dolocretes has been attributed to similar formation mechanisms of calcretes. Several processes to generate near-surface and soil-related dolomite accumulations by increasing Mg/Ca ratio of phreatic solutions have been suggested: (1) mixing of saline brines and fresh groundwater (El-Sayed et al., 1991; Colson and Cojan, 1996); (2) calcite precipitation from nearby groundwater resulting in Ca^{2+}-depleted but Mg^{2+}-enriched groundwater (Hutton and Dixon, 1981; Spötl and Wright, 1992; Armenteros et al., 1995); and (3) fluid movements through Mg-rich clays (Pimentel et al., 1996). Examples of phreatic dolocretes in Permo-Triassic fluvial sediments have been reported in the Paris Basin (Spötl and Wright, 1992), Sherwood Sandstones in the Corrib Field (W Ireland; Schmid et al., 2004, 2006), Wessex basin (S England; Mader, 1986; McKie et al., 1998), Abo-Tubb interval (NE New Mexico, USA; Kessler et al., 2001), Orenburg region (South Urals, Russia; Kearsey et al., 2012) and Argana Basin (Brown, 1980), among others.

Deposits generated above mean channel depth in fluvial systems (floodplain sediments and paleosols–calcrete and dolocretes) are prone to be incised and eroded during channel migration and base-level fall (Miall, 2006). Then, these penecontemporaneus reworked grains become part of fluvial sandstone framework as intrabasinal components, being called as “intraclast” or “rip-up clasts”. They usually concentrate in particular depositional facies such as channel-lags

* Corresponding author. Tel.: +34 958 246284.
E-mail addresses: shenares@ugr.es (S. Henares), arribas@ucm.es (J. Arribas), cultrone@ugr.es (G. Cultrone), viseras@ugr.es (C. Viseras).

http://dx.doi.org/10.1016/j.sedgeo.2016.03.020
0037-0738/

deposits (Allen and Wright, 1989; Garzanti, 1991). Its grain size distribution, mostly greater than other framework components according to their lower density (Zuffa, 1980, 1985), may result in a significant volume of sandstone framework represented by such clasts. Thus, rip-up clast occurrence has an important significance on paleoclimatic and paleogeographic reconstructions, by testifying the existence of coeval primary dolocretes, preserving provenance signature of intrabasinal sediments (Garzanti et al., 1989; Garzanti, 1991; Odin, 1985; Zuffa, 1980, 1985; Purvis and Wright, 1991; Spötl and Wright, 1992). In addition, there are evidences of the impact exerted by these grains on diagenetic evolution of host sandstones and, eventually, on reservoir quality through: (i) favoring mechanical compaction with a consequent drastic loss of intergranular space (Rittenhouse, 1971; Pittman and Larese, 1991; Gluyas and Cade, 1997; Paxton et al., 2002; Mousavi and Bryant, 2013); and (ii) sourcing eodiagenetic carbonate cements that reduce original porosity (Burley, 1984; Schmid et al., 2004, 2006; Morad et al., 2010; De Ros and Scherer, 2012).

On the basis of the double applied interest of rip-up clasts, occurrence and abundance of different types of such grains in Triassic fluvial deposits of Argana Basin (S Morocco; Fig. 1A) provide a great scenario to evaluate these questions. Thus, by coupling high-resolution petrographic and chemical analysis, this paper aims at: 1) characterizing origin and source of such clasts; and 2) evaluating their impact on host sandstones postdepositional evolution by examining their behavior during diagenesis. The proved correlation between the Argana Basin and the hydrocarbon-bearing Bay of Fundy Basin in Nova Scotia (Canada; Smoot and Castens-Seidell, 1994; Olsen, 1997; Calder et al., 1998; Hofmann et al., 2000; Letourneau and Olsen, 2003) reveals the relationship between spatial distribution of the different rip-up clast types and depositional facies as particularly interesting for a better understanding of fluid flow heterogeneity and reservoir compartmentalization.

2. Geological setting

The Triassic Argana Basin is located in the Western High Atlas of Morocco and is up to 20 km in width and extends over 85 km (Fig. 1A). It forms the eastward extension of the hydrocarbon-bearing Essaouira Basin (Medina, 1988; Broughton and Trépanier, 1993; Ellouz et al., 2003) which corresponds to the conjugate Atlantic passive continental margin of the Bay of Fundy Basin in Nova Scotia, Canada (Calder et al., 1998; Olsen et al., 2000; Letourneau and Olsen, 2003). Both basins show remarkable similarities in sedimentary facies and stratigraphy throughout their thick Late Permian–Early Jurassic successions suggesting a predrift proximity (Fig. 1B; Smoot and Castens-Seidell, 1994; Kent et al., 1995; Olsen, 1997; Hofmann et al., 2000). In Argana Basin, estimated maximum burial depth is about 1600–2000 m with a maximum temperature at the base of the stratigraphic sequence (ca. 6000 m thick) ranging between 150 and 250 °C (Leikine et al., 1996). Hydrothermal processes are not completely discarded by some authors (Lahcen et al., 2007). Argana Basin consists of a half-graben basin with 5–30° tilted blocks towards the NW that has experimented two main phases of extension, influencing sediment distribution patterns (Brown, 1980; Medina, 1991, 1995). First (pre-rifting) phase of extension only affected deposition of Late Permian sediments (Medina, 1991, 1995) whereas the second phase is considered coeval to Triassic deposition (syn-rift) by some authors (Brown, 1980; Laville and Petit, 1984; Medina, 1991, 1995) or later to that time (post-rift) by others (Hofmann et al., 2000; Baudon et al., 2012).

At the end of the Triassic, Argana and Fundy Basins were situated in the subtropical belt at about 20°N paleolatitude, where deposition took place under semi-arid to arid climates (Hay et al., 1982). In the Argana Basin, a long-term change in paleoclimate that ranges from semi-arid conditions with seasonal precipitation (Early to Middle Triassic) towards an arid, non-seasonal climate (Late Triassic) is preserved within the sedimentary cycles developed during several million years (Hofmann et al., 2000). A short-lived event of increased precipitation within the general trend of aridification is identified during the Carnian Pluvial Episode (Arche and López-Gómez, 2014 and references therein).

2.1. Stratigraphy

Continental red beds of the Argana Basin are represented by a ca. 5000-m-thick succession of Permo-Triassic sedimentary rocks (Tixeront, 1973, Brown, 1980) capped by the Argana basalt (205 ± 16 Ma; Fiechtner et al., 1992; Fig. 2). This stratigraphic succession is

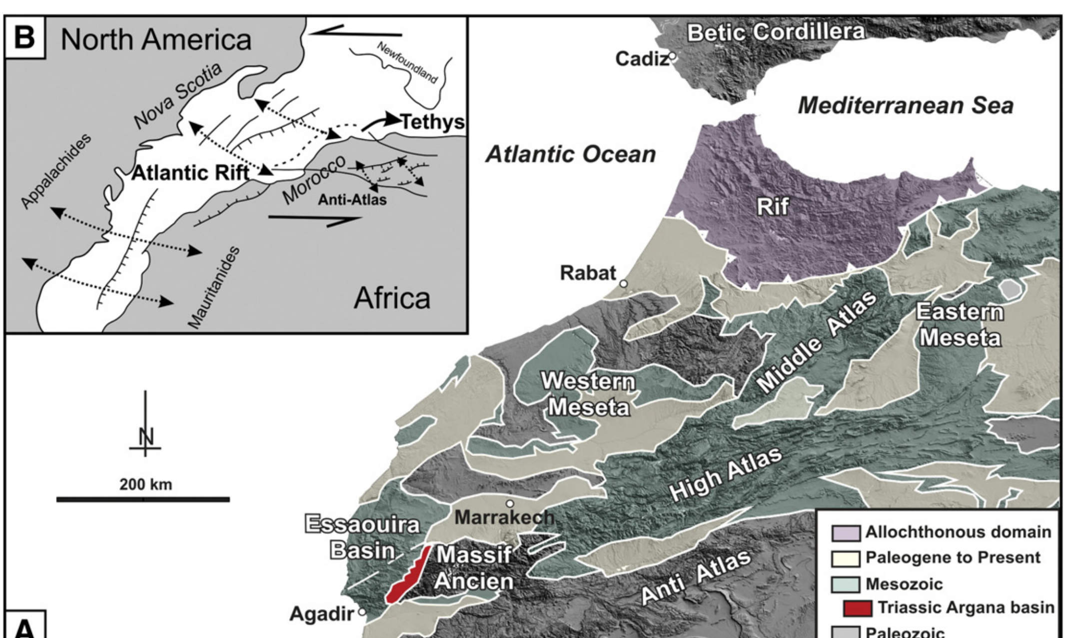

Fig. 1. A) Geological map of Western High Atlas showing present location of the study area. B) Paleogeographic map of Morocco at Triassic time (modified after Laville and Pique, 1991).

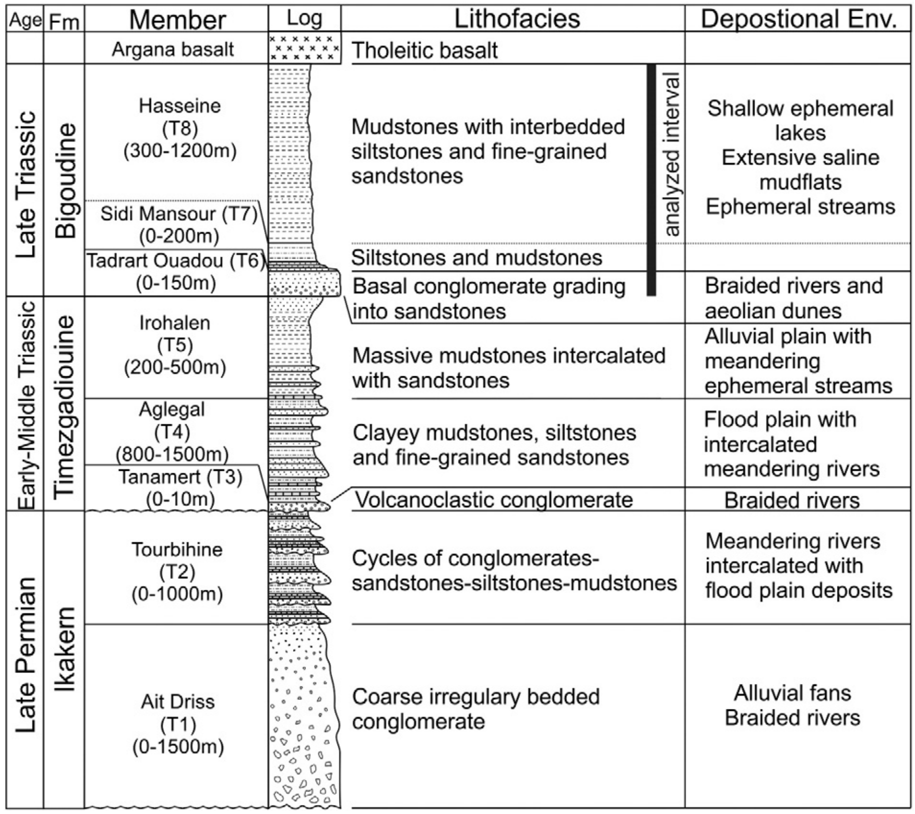

Fig. 2. Simplified lithostratigraphic log for the Permian and Triassic record in Argana Basin, showing the analyzed stratigraphic interval (modified after Tixeront, 1973; Brown, 1980; Hofmann et al., 2000). Thicknesses are maxima.

subdivided into eight lithostratigraphic units or members (namely T1 to T8; Tixeront, 1973) grouped into three formations (Brown, 1980). The lowermost Ikakern Fm (Late Permian, Brown, 1980; Jalil and Dutuit, 1996) rests unconformably on Palaeozoic basement and includes Ait Driss (T1) and Tourbihine (T2) members. It typically consists of alluvial fan conglomerates, grading vertically and laterally into cycles of conglomerate–sandstone–siltstone–mudstone from meandering rivers intercalated with floodplain deposits (Brown, 1980). The intermediate Timesgadiouine Fm (Early–Middle Triassic, Klein et al., 2011) overlies unconformably the Ikakern Fm and consists at its base on the Tanameurt Mb (T3), a volcanoclastic sheet-like conglomerate body of braided river origin (Brown, 1980). Aglegal Mb (T4) is dominated by clayey mudstones, siltstones and, in minor extent, fine-grained sandstones deposited in a flood plain/playa environment with development of vertisols and intercalations of meandering fluvial deposits (Brown, 1980; Hofmann et al., 2000). Irohalene Mb (T5) is characterized by sandstones cyclically intercalated with massive mudstones, generated on an alluvial plain setting with meandering ephemeral streams (Hofmann et al., 2000). The upper Bigoudine Fm (Late Triassic, Fiechtner et al., 1992) encompasses the Tadrart Ouadou Mb (T6) at the base, the Sidi Mansour (T7) and the Hasseine Mbs (T8) (Tixeront, 1973; Brown, 1980). The Tadrart Ouadou sandstone is interpreted as the result of the aforementioned Carnian Pluvial Event (Arche and López-Gómez, 2014) and is continuous throughout the Argana Basin. This unit consists in proximal braided river conglomerates grading upward into sand-dominated, distal braided river deposits with intercalated aeolian sandstones (Hofmann et al., 2000; Mader and Redfern, 2011). Both T7 and T8 are composed of similar, cyclically arranged mud-rich facies difficult to be separated into two distinctive members. T7/T8 strata formed in shallow ephemeral lakes and extensive saline mudflats with periodic fluvial and aeolian inputs of sand (Hofmann et al., 2000).

2.2. Depositional facies

For the purpose of this study, two fluvial systems are analyzed: the braided system corresponding to the Tadrart Ouadou Mb (T6 unit) and a straight channel from the Sidi Mansour-Hassein interval (T7/T8 unit).

The braided system from Tadrart Ouadou Mb was characterized in two different outcrops, 6 km apart approximately (Fig. 3A and B), to target its main depositional environments: main channel, lobate unit bars, compound bars and secondary channels. In one of the outcrops, cross-bedded sandstones with up to 2 m thick cross-bed sets are recognized with abundant rip-up clasts accumulated at the toes of cross-bedded sandstones (Fig. 3A). They correspond to foresets of megaripples and dunes developed at the tail of lobate unit bars that cover channel erosive bases (Lunt et al., 2004). Lateral and downstream accretion of lobate unit bars results in a larger-scale compound bar (Bridge et al., 1998; Lunt et al., 2004). This facies association is representative of a deep perennial braided system comprising multistorey fills with both lateral and vertical aggradation (Viseras and Fernández, 2010; Mader and Redfern, 2011). A main channel segment may become partially disconnected due to bank attachment processes, when bars migrate obliquely respect to the main current direction, being reduced to a secondary channel (Lunt et al., 2004). Secondary channel fills are characterized by a fining upward succession comprising epsilon cross-bedded sandstone with abundant rip-up clasts at the base, to cross- and ripple-laminated sandstone with flaser and wavy structures at the top (Fig. 3A). In the other outcrop, lowermost part shows meter-thick sets of planar cross-bedded and horizontal laminated sandstones with several tens of meters in lateral extension (Fig. 3B). Top is marked by an erosional-base channelized deposit with abundant rip-up clasts (Fig. 3B). Internal architecture and the occurrence of internal erosion

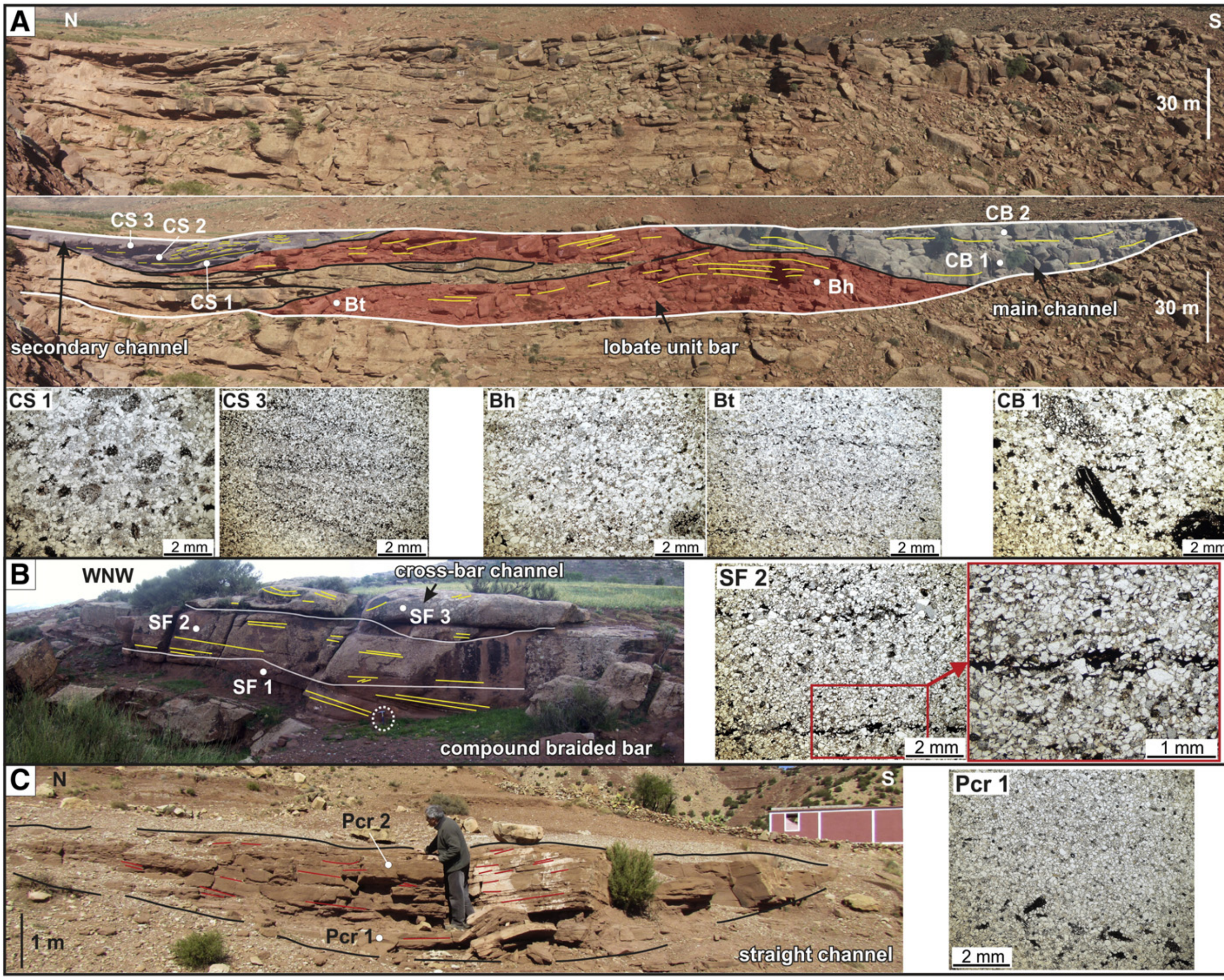

Fig. 3. Outcrop photointerpretations with analyzed depositional facies and sample location together with photomicrographs of the main textural features (plane-polarized light, PPL). A) Main braided channel (base and top; CB1 and CB2, respectively) along with adjacent lobate unit bars (bar-head and bar-tail; Bh and Bt, respectively) and associated secondary channel (base, mid and top; CS1, CS2 and CS3, respectively). B) Compound braided bar (lower-implantation- and middle-accretion-parts; SF1 and SF2, respectively) and its cross-bar channel (SF3). C) Straight channel (base and top; PCr1 and PCr2, respectively).

surfaces and rip-up clasts point out to a compound braided bar-type deposit (Viseras and Fernández, 2010) truncated by a cross-bar channel (Bridge et al., 1998).

Fluvial deposit from the T7/T8 interval is characterized by a 2 m-thick sandstone, with alternations of mudstone layers, that shows vertical aggradation (Fig. 3C). From the base to the top, a planar cross-bedding structure evolves to trough cross-bedding. Sedimentary architecture, dimension and internal structures suggest a straight channel as the fluvial depositional system (Viseras and Fernández, 2010, Viseras et al., 2011).

3. Methodology

A total of twelve sandstone samples from unweathered outcrop portions were analyzed which correspond to four fluvial depositional environments: (1) main braided channel (and adjacent lobate unit bars; Fig. 3A); (2) associated secondary channel (Fig. 3A), all in the first outcrop of T6 unit; (3) compound braided bar and its cross-bar channel (Fig. 3B) in the second outcrop of T6 unit; and (4) straight channel (Fig. 3C) of T7/T8 interval.

High-resolution petrographic analysis was performed including a special characterization and classification of the rip-up clasts according to their petrographic features and diagenetic behavior. Analysis was carried out on polished thin sections and freshly broken surfaces by using optical and field emission scanning electron microscopes (FESEM Gemini of Carl Zeiss SMT) equipped with an energy dispersive X-ray spectrometer. Cold-cathodoluminescence (CL) allowed to examine textural features and relationship between rip-up clasts and carbonate cements. Samples were etched and stained with hydrofluoric acid and Na-cobaltinitrite for plagioclase and K-feldspar identification, and with alizarin red-S and potassium ferricyanide for carbonate type discrimination. Gazzi-Dickinson (600 points per thin section) (Ingersoll et al., 1984; Zuffa, 1985, 1987) and grain size (100 grains per thin section) point-countings provided qualitative and quantitative data on framework composition and interstitial component to characterize depositional and diagenetic fabrics (Table 1). Intergranular volume (IGV), porosity loss by compaction and cementation (COPL and CEPL, respectively) as well as compactional index (I_{comp}) were calculated following established conventions (Table 1; Lundegard, 1992). Chemical composition of carbonates within rip-up clast and cements was determined on selected representative samples that contain higher amount of both types. Ca, Mg, Mn, Fe, Sr, and Ba contents were obtained by using a Cameca SX100 electron microprobe operating at 15 kV and 20 nA with an electron beam of 5 μm diameter.

Table 1
Petrographic data base of framework and interstitial components in analyzed sandstones, including main compositional and diagenetic indexes.

Unit	T6										T7/T8	
Depositional env.	Channel + Lobate unit bar				Slough channel			Compound bar			Straight channel	
Sample	CB1	CB2	Bh	Bt	CS1	CS2	CS3	SF3	SF2	SF1	PCr1	PCr2
Framework												
Qm	286	320	330	309	257	296	319	305	321	353	352	371
Qp	45	42	39	52	38	43	18	52	29	54	40	40
K	42	41	27	29	8	49	27	18	24	20	13	16
K replaced by clays	1	4		6		1	3	1	3		1	1
P	21	24	14	20	9	20	43	22	27	18	8	18
P replaced by clays	3	8	5	6	1		8	1	7	2	4	4
Phyllite	5	5	10	11	2	6	16	7	9	5	27	44
Schist	2	1	2	4	1		3	2	2	1	7	16
Siltsonte	1		5	1	1				16			
Sandstone					6			2	1	1	3	3
Muscovite	2	5	2	12	2	3	5	1	2	2	1	2
Chlorite											1	2
Opaque	4	4	6	4	2	5	2	1	3		1	6
Turmaline		2				1	2				1	
Zircon	2		1				2				1	
Rutile	1					1						
Epidote	1	2			1	1	1	2			1	2
Glauconite											1	1
Muddy RuC[a]	88	77	59	70	24	50	48	20	56	38	8	2
Dolomitic muddy RuC	13				24	20	13	4	4	3	6	2
Dolomite crystalline RuC	4	2	9		89	19	14	12	4	2	7	3
Intergranular space												
Feldspar overgrowth	2	1	1	2	2	3		1	1	2	1	3
Quartz overgrowth	40	28	37	33	29	20	6	30	47	47	20	13
Dolomite	30	24	47	15	99	55	70	61	21	30	70	30
Calcite								63	9	8	4	1
Primary porosity	3	5	6	20	5	7		5	14	17	29	18
Total	596	600	600	600	600	600	600	610	600	603	607	600
IGV[b]	12.7	9.7	14.6	12.5	18.8	14.2	9.5	18.8	15.0	17.2	21.3	11.6
COPL[b]	31.3	33.6	29.7	31.4	26.1	30.1	33.7	25.9	29.4	27.5	23.7	32.1
I_{comp}[b]	0.8	0.9	0.8	0.8	0.7	0.8	0.8	0.7	0.8	0.7	0.7	0.8
Q[c]	81.7	81.5	85.3	82.4	91.5	81.7	77.1	87.1	79.7	89.6	86.2	80.1
F[c]	16.4	17.1	10.7	13.9	5.5	16.9	18.5	10.2	13.9	8.8	5.7	7.6
R[c]	2.0	1.3	4.0	3.7	3.0	1.4	4.3	2.7	6.4	1.5	8.1	12.3
Qm[d]	80.8	80.6	87.5	83.5	93.4	80.9	79.8	87.9	84.0	89.8	93.1	90.5
K[d]	12.3	11.3	7.4	9.5	2.9	13.7	7.5	5.5	7.1	5.1	3.7	4.1
P[d]	6.9	8.1	5.2	7.0	3.6	5.5	12.8	6.6	8.9	5.1	3.2	5.4
Mean grain size (mm)	0.27	0.19	0.26	0.18	0.29	0.25	0.1	0.3	0.22	0.2	0.18	0.17

[a] RuC: rip-up clast.
[b] IGV: intergranular volume, COPL: compactional porosity loss, I_{comp}: compactional index (Lundegard, 1992).
[c] Q: total quartz, F: total feldspar, R: total rock fragments (Pettijhon et al., 1973).
[d] Qm: monocrystalline quartz, K: K-feldspar, P: plagioclase (Dickinson, 1985).

4. Results

4.1. Host sandstone detrital fabric

Grain size ranges from very-fine to medium-grained sand with moderately to well-sorted, subrounded to subangular grains. Mean grain size varies within each depositional environment according to depositional facies. In the main channel and adjacent lobate unit bar, mean grain size decreases, vertically, from channel-lag deposit (0.27 mm) to channel top (0.19 mm) and, laterally, from bar-head (0.26 mm) to bar-tail (0.18 mm) (Fig. 3A). In associated secondary channel, there is a fining upward succession from basal channel-lag (0.29 mm) to epsilon cross-beds (0.25 mm) and ripple cross lamination at the top (0.1 mm) (Fig. 3A). In the compound braided bar, mean grain size increases from the base of the bar (0.2 mm) upwards (0.22 mm), being coarsest at the cross-bar channel (0.3 mm). In the straight channel, mean grain size slightly decreases upwards (from 0.18 to 0.17 mm). Depositional texture, far to be uniform at thin section scale, usually displays sedimentary structures such as parallel and ripple cross lamination highlighted by laminae with higher rip-up clast content (Fig. 3A to C) or alternation of laminae with different grain sizes (Fig. 3A, Bh sample).

Compositional signature classifies sandstones mainly as extraclastic arenites (Fig. 4A; according to Zuffa, 1980) with subarkosic composition in samples from braided fluvial system (average $Q_{83.8}F_{13.2}R_3$) and sublitharenitic composition in samples from straight channel (average $Q_{83.1}F_{6.7}R_{10.2}$) (Table 1; Fig. 4B). Non-undulatory monocrystalline quartz is the dominant grain type followed by polycrystalline quartz without tectonic fabric and, in minor extent, inherited quartz (i.e. quartz with rounded overgrowths). Feldspars consist of K-feldspars and plagioclases in similar proportions that barely vary among different facies (total average of $Qm_{84.8}K_{8.2}P_7$ in T6 braided system and $Qm_{91.8}K_{3.9}P_{4.3}$ in T7/T8 straight channel; Fig. 4C). Rock fragments are represented in order of abundance by low-, medium-grade metamorphic (phyllites and schists) and sedimentary (sandstones and siltstones) grains. Other extrabasinal components in accessory content are micas, mainly muscovite, and silt-sized, well-rounded heavy minerals (zircon, tourmaline, rutile, epidote and opaques; 0–1.6%). Intrabasinal components may amount to an important portion of framework. They are substantially represented by different rip-up clast types (up to 29.2%; see next section for further characterization) and, subordinate, by well-rounded glauconite with similar size of other accessory host framework grains (0.2%).

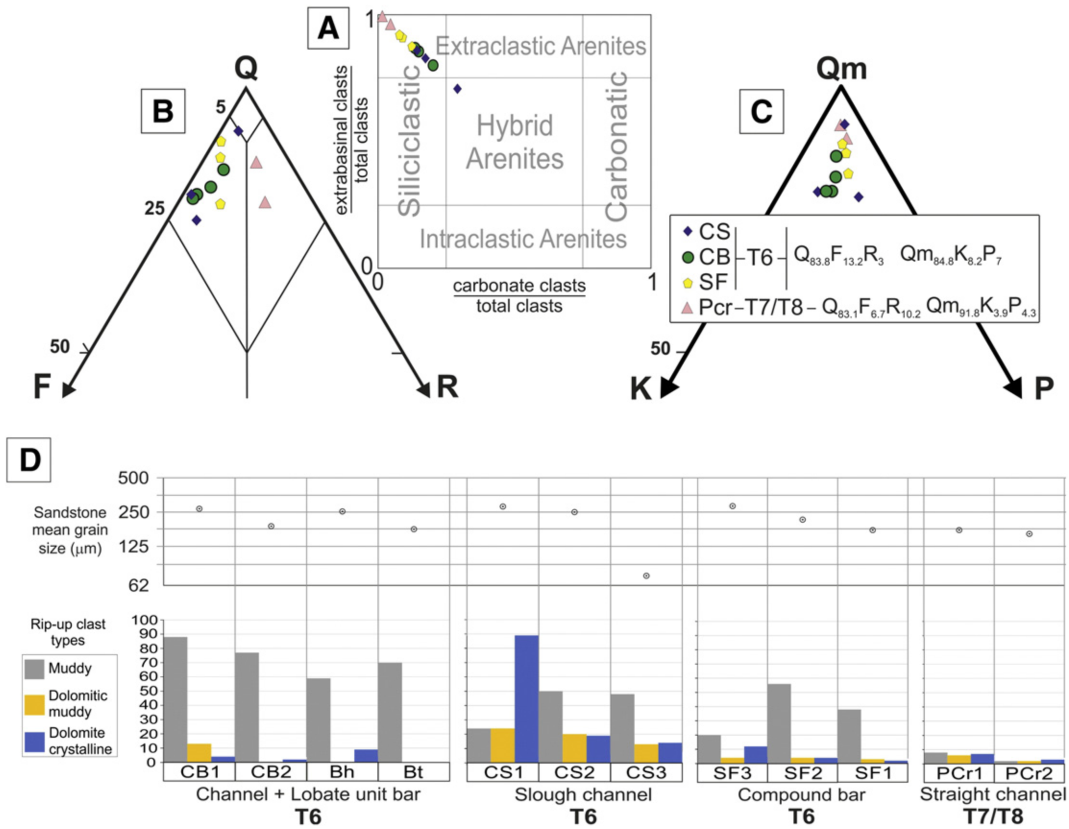

Fig. 4. Main compositional features of framework sandstones. A) Genetic (extrabasinal clasts/total clasts) versus mineralogical (carbonate clasts/total clasts) signatures (according to Di Giulio and Valloni, 1992). B) QFR ternary diagram: Q: total quartz; F: total feldspars; R: total rock fragments (after Pettijohn et al., 1973). C) QmKP ternary diagram: Qm: total monocrystalline quartz; K: total monocrystalline K-feldspar; P: total monocrystalline plagioclase (after Dickinson, 1985). D) Abundance of different rip-up clast types according to depositional facies and grain size.

4.2. Rip-up clast characterization

Rip-up clasts occur in all analyzed sandstones (Fig. 4D) and their size decreases as grain size does according to depositional facies. On the basis of their petrographic features (rip-up clast composition: inclusion or not of dolomite crystals and, if so, its abundance and size) and their mechanical behavior (ductile, semi-ductile and rigid), the following three main classes of rip-up clasts are differentiated:

1) Muddy rip-up clasts. They are dark red in color due to Fe-oxide presence and are composed by clay minerals, mainly illite from EDX analyses (Fig. 5A). They occur in all depositional facies with a general trend of increasing abundance in coarser facies from main braided and straight channels. Opposite trend is observed in associated braided secondary channel and compound bar environments (Fig. 4D). They usually concentrate in preferential laminae according to sedimentary structure (Fig. 3B). Size ranges from 0.1 to 5 mm. This rip-up clast type displays a highly ductile behavior during mechanical compaction which deforms and squeezes them between other rigid framework grains (Fig. 5A).
2) Dolomitic muddy rip-up clasts. They are composed by dolomite crystals embedded in a clayey matrix with similar characteristics to that of muddy rip-up clasts (Fig. 5B and C). Inclusion of silt-sized siliciclastic grains is rare. Dolomite occurs as euhedral rhombic crystals, some of them with a clean outer rim (Fig. 5B) that appears as a slight zonation at SEM (Fig. 6A and B). Most of dolomite crystals contain red-colored inclusions, some with a radial pattern from the central crystal area until the clean rim (Fig. 5B). Dolomite abundance within the clast varies between 10% and 50% of total clast volume. Crystal size is highly variable among crystals of different clasts, ranging from 0.05 to 0.1 mm, and does not show an apparent relationship with clast size (0.3–0.9 mm). Abundance of this rip-up clast type decreases according to grain size in each depositional environment, being absent in some facies of channel and adjacent lobate unit bar (Fig. 4D). Their spatial distribution does not follow sedimentary structure. These rip-up clasts display a semi-ductile behavior during diagenesis, being partially deformed by mechanical compaction (Fig. 5B and C).
3) Dolomite crystalline rip-up clasts. They are usually composed by dolomite crystals with minor amounts of intercrystalline clayey matrix (Fig. 5D and E), similar to that of muddy rip-up clasts. In other cases, they are exclusively composed of crystalline dolomite constituting an idiotopic mosaic (Fig. 5F and G). Inclusion of siliciclastic grains is common and, sometimes, abundant. Dolomite crystal habit is analogous to that of the dolomitic muddy rip-up clasts, including clear outer rims and inclusions (Fig. 5D, E and H; Fig. 6B). Subhedral and anhedral habits with nonplanar, highly irregular intercrystalline boundaries are also present (Fig. 5E). Dolomite abundance within the clast varies between 50% and 100% of total clast volume. Dolomite crystal size is highly variable between crystals from the same clast and crystals from different clasts, ranging from dolomicrite textures (Fig. 5G) up to 0.2 mm, without an apparent relationship with clast size (0.3–3 mm). These rip-up clasts are mainly equidimensional and may show organic structures filled by inherited dolomite cement (Fig. 5H). Abundance of dolomitic crystalline rip-up clasts decreases as grain size does in each depositional environment, being especially abundant as channel-lag deposits (Fig. 4D). This rip-up clast type behaves as rigid grains, non-deformed by mechanical compaction, preserving its original grain shape (Fig. 5D to G).

Under CL, dolomite crystals within rip-up clasts are systematically bright orange luminescent (Fig. 6D to H). Euhedral rhombic dolomites

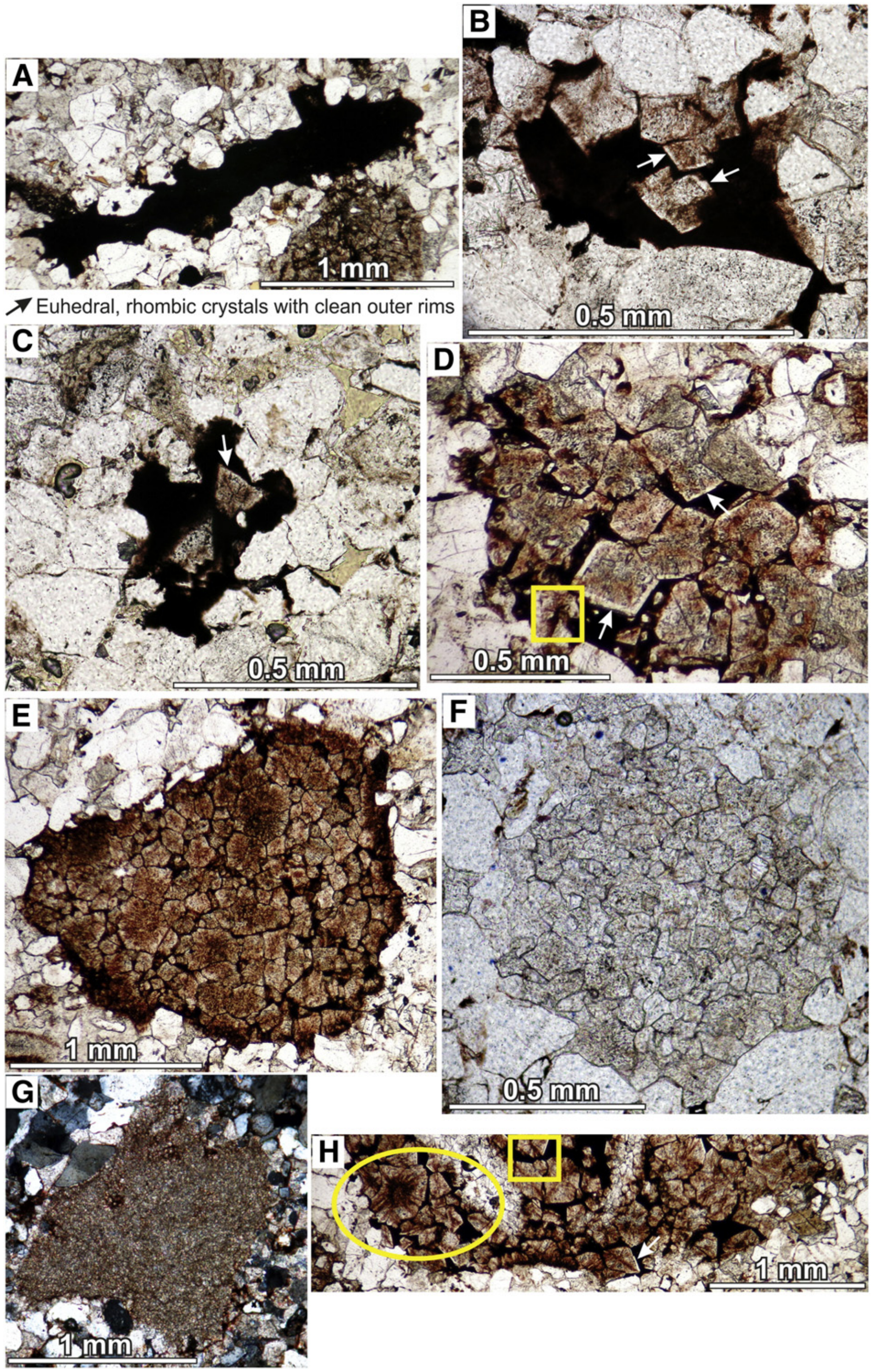

Fig. 5. Photomicrographs showing the different rip-up clast types. A) Muddy rip-up clast strongly deformed by mechanical compaction (CB1 sample). B and C) Dolomitic muddy rip-up clasts partially deformed by mechanical compaction (CS2 and CS1 samples, respectively). Notice clean outer rims in dolomite crystals. D) Dolomite crystalline rip-up clast composed by euhedral, rhombic dolomite crystals with clean outer rims and radial-pattern inclusions, embedded in a clayey matrix (CS1 sample). The yellow box area corresponds to SEM image of Fig. 6A. E) Dolomite crystalline rip-up clast composed by dolomite crystals with nonplanar intercrystalline boundaries and radial-pattern inclusions, embedded in a clayey matrix (SF3 sample). F and G) Dolomite crystalline rip-up clasts exclusively composed by dolomite crystals constituting meso- and microcrystalline idiotopic mosaics, respectively (SF3 and Bh samples, respectively). H) Dolomite crystalline rip-up clast composed by dolomite crystals with clean outer rims and radial-pattern inclusions, embedded in a clayey matrix (CS1 sample). Organic structures within the clasts (light areas) are filled by inherited dolomite cement. The yellow box area corresponds to SEM image of Fig. 6B. Circle area corresponds to CL photomicrograph of Fig. 6F. (All photomicrographs in plane-polarized light, PPL, except G in cross-polarized light, XPL).

with clear outer rims show a slight zonation from darker orange cores to brighter yellowish orange rims (Fig. 6D, E and F). Inherited dolomite cement within dolomitic crystalline rip-up clasts may present the same zonation (Fig. 6F). Bright orangish yellow luminescent inclusions are observed within dolomite crystals (Fig. 6C and D) whereas those of radial pattern and red-colored at optical microscope luminesce darker orange (Fig. 6C to F).

Microprobe analysis indicates that dolomite crystals within rip-up clasts are approximately stoichiometric (total average CaO = 50.09% wt.; MgO = 48.55% wt.) with relative high Mn and Fe contents (total

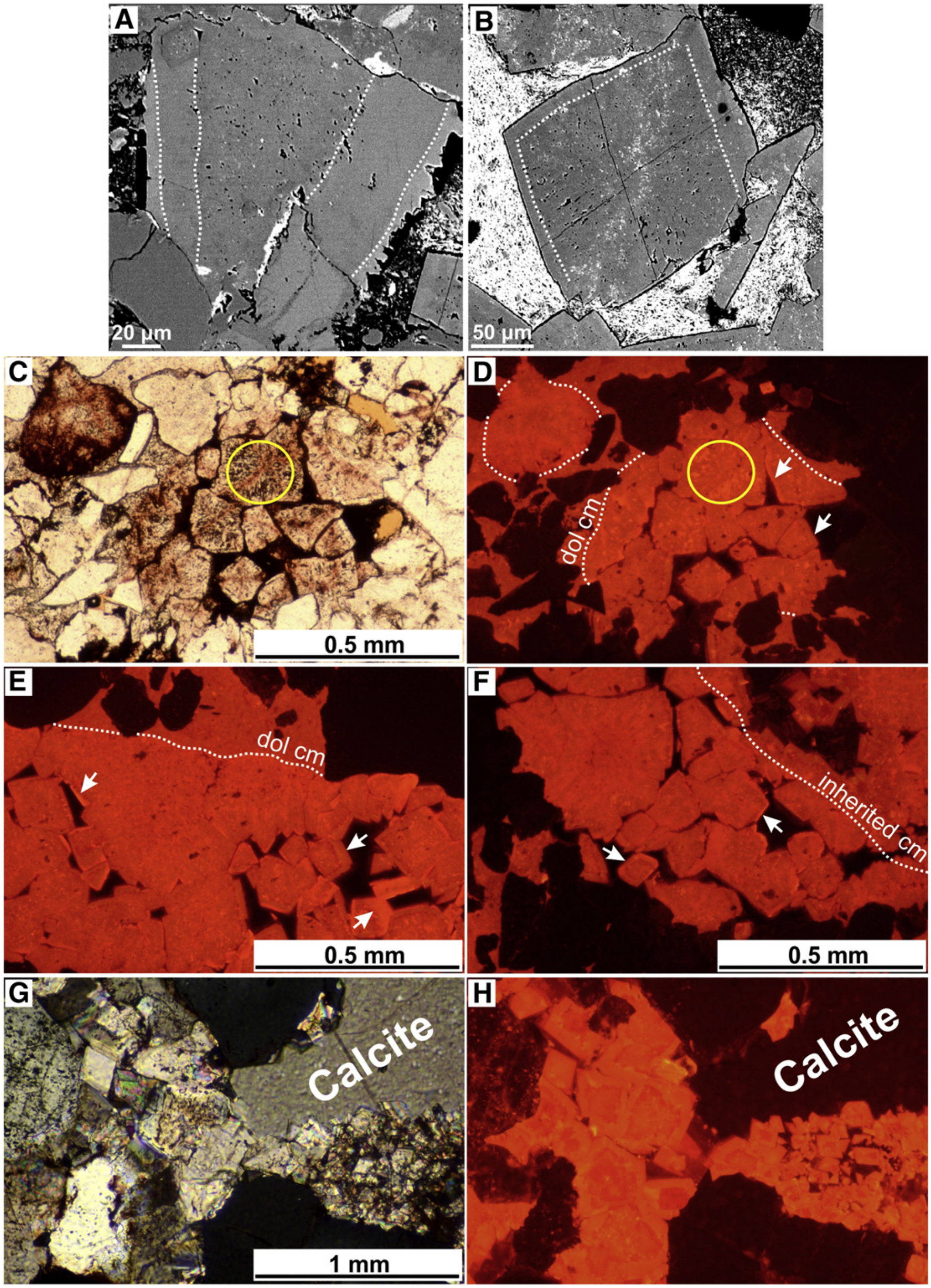

Fig. 6. A and B) SEM images of euhedral dolomite crystals with zonation from central areas to clearer outer rims, in both cases (dotted lines), and bright inclusions and clayey matrix due to the presence of Fe-oxides, in B. C and D) Same microphotograph under PPL and CL showing luminescence difference between dolomite crystal within rip-up clasts (bright orange luminescent) and poikilotopic dolomite cement (slightly darker; dol cm). Clear outer rims (arrows) luminesce brighter yellowish orange. Black-colored inclusions under PPL are bright orangish yellow luminescent whereas those red-colored are darker orange (solid circle) (CS1 sample). E) CL microphotograph corresponding to circle area of Fig. 9C showing luminescence difference between dolomite crystal within rip-up clasts (bright orange luminescent) and syntaxial dolomite cement (slightly darker; dol cm). Zonation of euhedral dolomite crystals from darker cores to brighter rims is also observed (arrows; CS1 sample). F) CL microphotograph showing the same zonation in inherited dolomite cement (inherited cm). Brighter yellowish orange luminescent rims (arrows) and darker orange luminescent inclusions within dolomite crystals are also recognizable. G and H) Same microphotograph under cross-polarized light (XPL) and CL showing difference between luminescent zoned dolomite cement and dull luminescent calcite cement (SF3 sample).

average Mn = 5532 ppm; Fe = 2146 ppm) (Fig. 7A and B) and low Sr (total average 358 ppm) and Ba (total average 132 ppm). Zonation in dolomite crystals, when occurs, is due to variations in Fe and Mn contents (core: Mn = 5677 ppm, Fe = 2340 ppm; rim: Mn = 5387 ppm, Fe = 1953 ppm; Fig. 7B). At SEM and under CL, clearer and brighter orange luminescent outer rims, respectively, are associated to

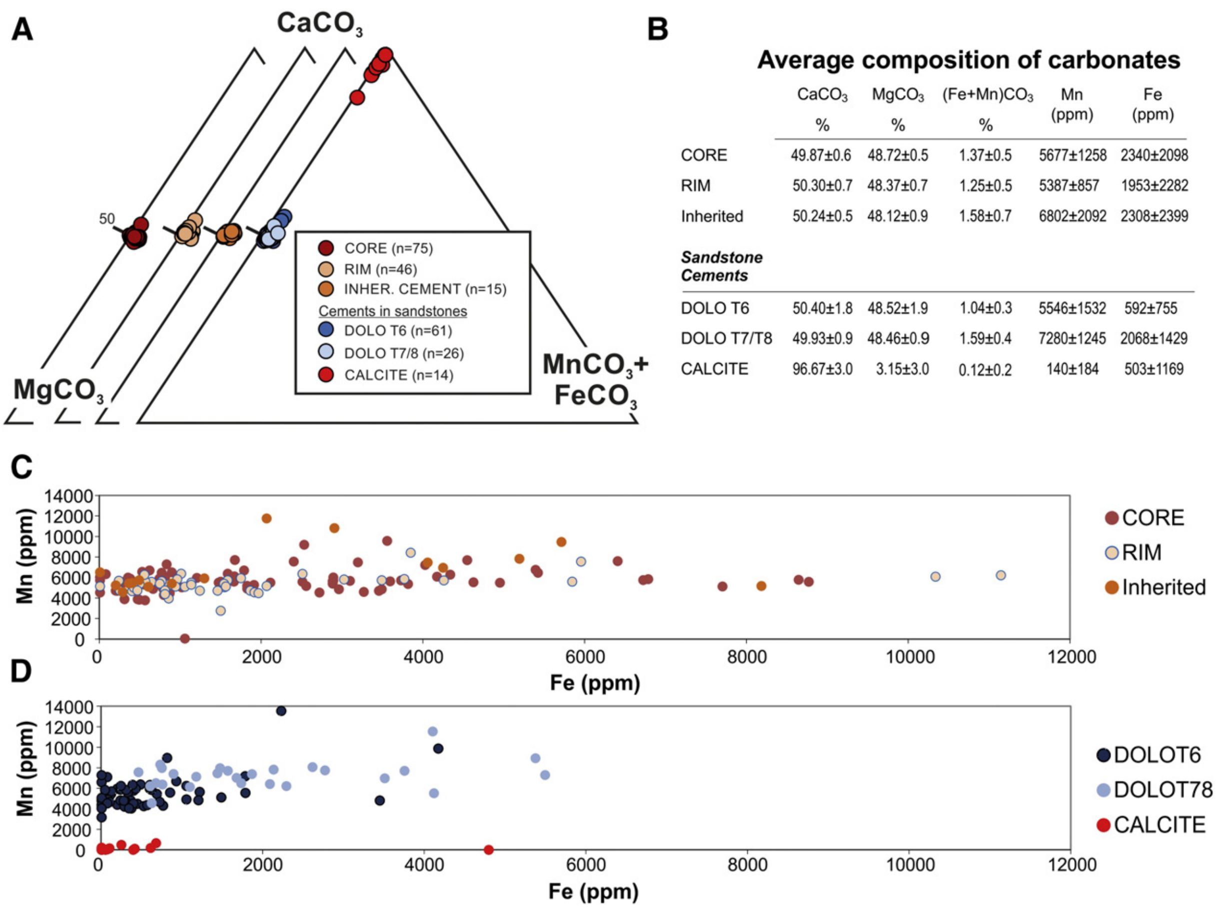

	$CaCO_3$ %	$MgCO_3$ %	$(Fe+Mn)CO_3$ %	Mn (ppm)	Fe (ppm)
CORE	49.87±0.6	48.72±0.5	1.37±0.5	5677±1258	2340±2098
RIM	50.30±0.7	48.37±0.7	1.25±0.5	5387±857	1953±2282
Inherited	50.24±0.5	48.12±0.9	1.58±0.7	6802±2092	2308±2399
Sandstone Cements					
DOLO T6	50.40±1.8	48.52±1.9	1.04±0.3	5546±1532	592±755
DOLO T7/T8	49.93±0.9	48.46±0.9	1.59±0.4	7280±1245	2068±1429
CALCITE	96.67±3.0	3.15±3.0	0.12±0.2	140±184	503±1169

Fig. 7. Carbonate chemical composition: CORE and RIM = core and rim of dolomite crystals within rip-up clasts, respectively; INHER. CEMENT = inherited dolomite cement within rip-up clasts; DOLO T6 and DOLO T7/T8 = dolomite cements from T6 braided system sandstones and T7/T8 straight channel sandstones, respectively; CALCITE = calcite cement from T6 sandstones in compound braided bar environment (SF samples). A) $CaCO_3$–$MgCO_3$–(Mn + Fe)CO_3 ternary diagrams showing almost stoichiometric compositions in all cases. B) Table summarizing average composition of carbonates for major elements. C) Fe versus Mn content in dolomite within rip-up clasts. Scatter of data shows a non-constant core-rim variation trend of these elements. D) Fe versus Mn content in sandstone carbonate cements. There is an increase in both element contents from T6 to T7/T8 dolomite cement.

both higher Mn and Fe contents (Fig. 6A to F). However, core-rim variation trend between these elements is highly irregular among dolomite crystals from the same rip-up clast as well as from different clasts. Combinations are variable from core to rim (Fig. 7C): Fe decreases whereas Mn increases (Fig. 6B), and vice versa, or both elements increase (Figs. 6A; 7C). Inherited dolomite cement within rip-up clasts is very similar in composition to dolomite crystals in terms of average CaO and MgO contents (50.24% and 48.12% wt.; Fig. 7A and B), with slightly higher Mn (6802 ppm), Sr (590 ppm) and Ba (510 ppm) contents but lower Fe (2308 ppm) (Fig. 7B and C).

4.3. Host sandstone diagenesis

Mechanical compaction dominates over chemical compaction and is the main porosity-reducing diagenetic process as indicated by an $I_{comp} < 0.5$ in all analyzed sandstones (Lundegard, 1992). It is manifested as mechanical deformation of ductile grains such as muddy and, in minor extent, dolomitic muddy rip-up clasts (Fig. 5A to C), medium-grade metamorphic lithic fragments and micas. Mechanical compaction is partially inhibited by early diagenetic cements which preserve intergranular volume (IGV). IGV is strongly facies-related with higher IGV values systematically associated to coarser grain sizes within each depositional environment (Fig. 8A). Highest IGV (IGV = 21.3%) is associated to straight channel base (PCr1 sample) whereas lowest IGV (IGV = 9.5%) is at secondary braided channel top (CS3 sample). Conversely, higher COPL values correspond mainly to finer-grained facies within each depositional environment (Fig. 8A).

The main porosity-modifying cements in sandstones include quartz (1–7.8%) and feldspar (0–0.5%) overgrowths and dolomite pore-filling cement (4–24.6%) (Fig. 9A to D). Calcite cement only occurs in compound braided bar depositional environment (SF samples; 1.3–9.8%). Feldspar overgrowths form thin and continuous euhedral prisms around detrital feldspar grains (Fig. 9A). It is the earliest cement being systematically overgrown by the rest of authigenic minerals (Fig. 8B). Dolomite replacement of this cement is common (Fig. 9A). Dolomite precipitates as: (i) coarse, euhedral, poikilotopic, and rhombic crystals (up to 3 mm; Fig. 9B) that preserve high IGV and, in some cases, inhibit quartz overgrowth formation; (ii) syntaxial dolomite that develops occluding sandstone intergranular space as overgrowths from rip-up clast dolomite crystals (Fig. 9C); and (iii) fine, euhedral (up to 0.05 mm), rhombic crystals in direct contact with detrital grains that preserve primary porosity (Fig. 9D). Last dolomite textural type only occurs in T7/T8 straight channel samples (PCr samples) where it represents the earliest cement that preserves highest IGV and primary porosity values (Fig. 8B). Under CL, poikilotopic and syntaxial dolomite cements show the same orange luminescent color than dolomite crystals within rip-up clasts, although slightly darker (Fig. 6D, E and F). Locally, euhedral dolomite cement may be zoned from darker cores to brighter orange luminescent rims (Fig. 6G and H). Quartz occurs as well-developed, euhedral prisms around detrital quartz grains with occasional bipyramidal habit (Fig. 9E) and, in minor amount, as microcrystalline rims (<10 μm) (Fig. 9F). Quartz, when it is not inhibited by dolomite cement, overlies dolomite crystals (Fig. 9G) and is postdated by calcite cement (Figs. 8B and 9H). Calcite forms poikilotopic pore-filling cement that

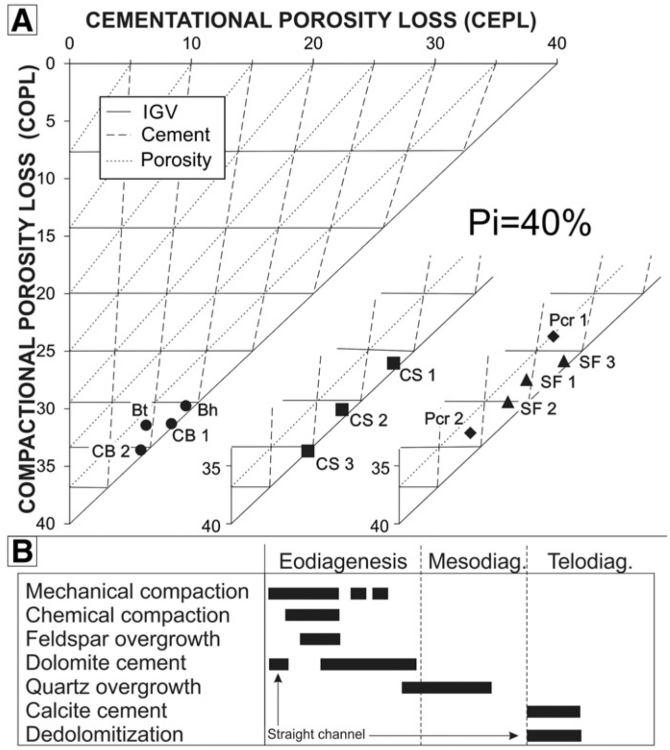

Fig. 8. Diagenetic evolution of host sandstones. A) Compactional (COPL) versus cementational (CEPL) porosity loss diagrams (modified after Lundegard, 1992). B) Diagenetic sequence of main diagenetic processes as interpreted from petrographic analysis.

systematically overlies the rest of cements (Figs. 9B and H; 8B). Under CL, calcite is dull luminescent (Fig. 6G and H). Other minor diagenetic processes encompass replacement of framework grains by carbonates (both dolomite and calcite), replacement of feldspars by phyllosilicates (mainly illite) and dedolomitization (only observed in samples from T7/T8 straight channel; Fig. 8B).

Chemical analysis of authigenic dolomite from both stratigraphic units (T6 and T7/T8) shows an important similarity in composition with dolomite crystals in terms of CaO and MgO contents (total average 50.17% wt. and 48.49% wt.; Fig. 7A and B). Differences with rip-up clast dolomite crystals as well as between dolomite cements from both units are mainly associated to Fe and Mn contents. Authigenic dolomite shows slightly higher Mn (6413 ppm, total average) but significantly lower Fe (1330 ppm, total average) contents than dolomite crystals within rip-up clasts (Fig. 7B and D) whereas, from braided system (T6 unit) to straight channel (T7/T8 unit), there is a general increase in both elements (T6: Mn = 5546 ppm and Fe = 592 ppm; T7T/8: Mn = 7280 ppm and Fe = 2068 ppm; Fig. 7B and D). Calcite cement is not purely stoichiometric due to MgO content (CaO = 96.67% wt.; MgO = 3.15% wt.). Fe, Mn and Ba are relatively low (503 ppm, 140 ppm and 48 ppm, respectively) whereas Sr content is the highest among all carbonates (600 ppm) (Fig. 7B and D).

5. Discussion

5.1. Origin of rip-up clasts

Rip-up clasts in fluvial sandstones from Argana Basin (T6 and T7/T8 stratigraphic units) have been considered as intrabasinal components according to following textural and compositional criteria (Zuffa, 1985; Garzanti, 1991): (1) grain size mostly greater than other framework grains; (2) inclusion, in a clayey matrix, of idiomorphic dolomite crystals with a wide range of crystal size and abundance; and (3) inclusion, in crystalline dolomite mosaic, of finer-grained siliciclastic grains (mainly quartz) than surrounding siliciclastic framework components. In addition, frequent irregular contours in muddy-dominated grains as result of mechanical compaction denote lack of lithification and thus absence of burial diagenesis in the original source. In fluvial systems, intrabasinal detrital products derived from low preservation potential sediments are mainly associated to erosion of floodplain subenvironments (Garzanti, 1991).

Cloudy cores in dolomite crystals with abundant radial-pattern inclusions of Fe-oxides and clay minerals point out to a first stage of replacive growth in a muddy matrix (Fig. 10A and B). Locally, a subsequent stage of displacive growth can be deduced from the presence of clean outer rims that deform muddy ground mass of host original sediments (Fig. 10C and D). Bright orange luminescence of dolomite crystals denotes slightly reducing conditions with incorporation of Mn^{2+} and Fe^{2+}. Slightly variations in chemical composition of dolomite crystals, which are approximately stoichiometric (Fig. 7A and B), suggest that dolomite does not result from dolomitization processes of previous calcite minerals (Hardie, 1987; Kupecz and Land, 1994). All these features are consistent with groundwater (phreatic) dolocretes embedded in muddy floodplain sediments as the source of different rip-up clast types (Arakel, 1986; Armenteros et al., 2003; Wright and Tucker, 1991; Spötl and Wright, 1992; Colson and Cojan, 1996; Pimentel et al., 1996). A vadose (pedogenic) origin for some of these dolocretes cannot be completely ruled out as it is suggested by the presence of organic structures with inherited dolomite cement within several dolomite crystalline rip-up clasts (Fig. 5H).

Genesis of groundwater dolocretes requires low sedimentation rates in evaporation-dominated floodplain environment (i.e. saline lakes) where groundwaters are depleted in Ca^{2+} as result of nearby calcrete formation (Andrews, 1985; Arakel, 1986; Arakel et al., 1989, 1990; Colson and Cojan, 1996; Khadkikar et al., 1998). Similar phreatic dolocretes have been documented in fluvial deposits where precipitation of evaporate minerals (gypsum) in playa-lake environment is the main factor of groundwater Ca-depletion (Arribas et al., 1996). Presence of coeval shallow ephemeral lakes and extensive saline mudflats during T6 and T7/T8 deposition has been reported by Brown (1980) and Hofmann et al. (2000).

Very early (pre-compactional), fine-grained, rhombic dolomite cement in straight channel samples (T7/T8 unit; Fig. 9D) may constitute an example of a phreatic dolocrete generated in a high porous media (Nash and McLaren, 2003). Morphology, abundance and size of dolomite crystals within dolocretes will depend on host rock lithology, porosity and permeability (Khalaf, 1990).

Similar muddy rip-clasts with dolomite crystals have been described in fluvial–aeolian sandstone reservoirs from Recôncavo Basin (Brasil) by De Ros and Scherer (2012). These authors interpret dolomite as replacement of rip-up clast during very early (pre-compactional) diagenetic stages. In the Argana Basin, the present study demonstrates that dolomite crystals are primary in origin and later reworked. In fact, its presence or not within rip-up clasts will have a major impact on diagenetic evolution of host sandstone.

5.2. Geochemical diagenetic processes in host sandstones

K-feldspar overgrowth is interpreted as the first cementing phase, resulting from alkaline (high aK^{+}/aH^{+}), silica-rich eodiagenetic waters commonly associated to early diagenetic stages in arkosic red beds (Waugh, 1978; Arribas, 1987; Morad et al., 1989). Dolomite cement, which locally replaces K-feldspar overgrowths, precipitates from alkaline phreatic waters with a high Mg/Ca ratio that may be derived from near-surface evaporitic processes during eodiagenesis (Hutton and Dixon, 1981; Spötl and Wright, 1992). This cement, in its several growth habits (poikilotopic, syntaxial and fine-grained rhombic crystals), occludes primary pores thus preventing intense mechanical compaction and predates quartz overgrowths. Silica for quartz cement may be partially released from weak chemical compaction processes during burial

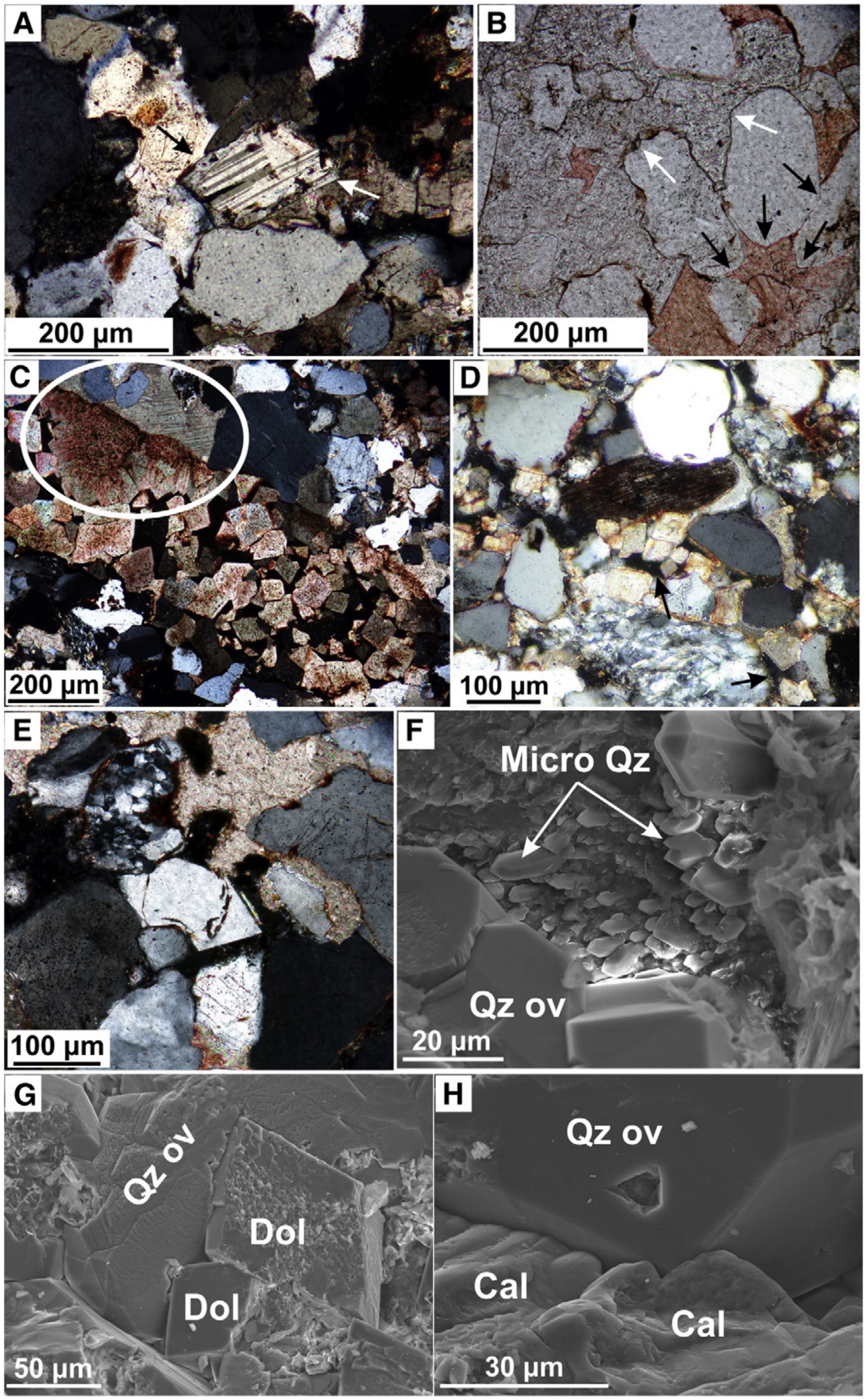

Fig. 9. Optical microphotographs and SEM images of main porosity-modifying cements affecting host sandstones. A) Feldspar overgrowth partially replaced by dolomite cement (white arrow) and postdated by quartz overgrowth (black arrow) (XPL, CS1 sample). B) Coarse, euhedral, poikilotopic dolomite cement inhibiting quartz overgrowth formation (white arrows). Notice the occurrence of well-developed quartz overgrowth in the same grains, postdated by calcite cement (black arrows) (PPL, SF3 sample). C) Syntaxial dolomite cement developed in adjacent intergranular space as overgrowths from rip-up clast dolomite crystals (circle area; XPL, CS1 sample). Circle area also corresponds to CL image of Fig. 6E. D) Fine, euhedral, rhombic crystals of dolomite cement preserving primary porosity (black arrows) (XPL, PCr1 sample). E) Well-developed quartz overgrowth with bipyramidal habit (XPL, SF3 sample). F) Microcrystalline rim of quartz overgrowths showing prismatic habits (Micro Qz). Coarser, euhedral quartz overgrowths are also observed (Qz ov) (CS2 sample). G) Quartz overgrowth overlaying dolomite cement (Dol) (CS1 sample). H) Quartz overgrowth postdated by calcite cement (SF2 sample).

diagenesis. Nevertheless, alteration of K-feldspar to illite and/or transformation of smectite into illite are also encouraged as sources of Si^{4+} (Worden and Morad, 2003) according to the sandstone framework composition and the presumable incorporation of smectitic clays in primary muddy rip-up clast composition. Both processes require high temperature diagenetic environments (130–140 °C; Bjørlykke, 1994) which is consistent with the maximum temperature data estimated for Argana Basin (150 °C; Leikine et al., 1996) without invoking

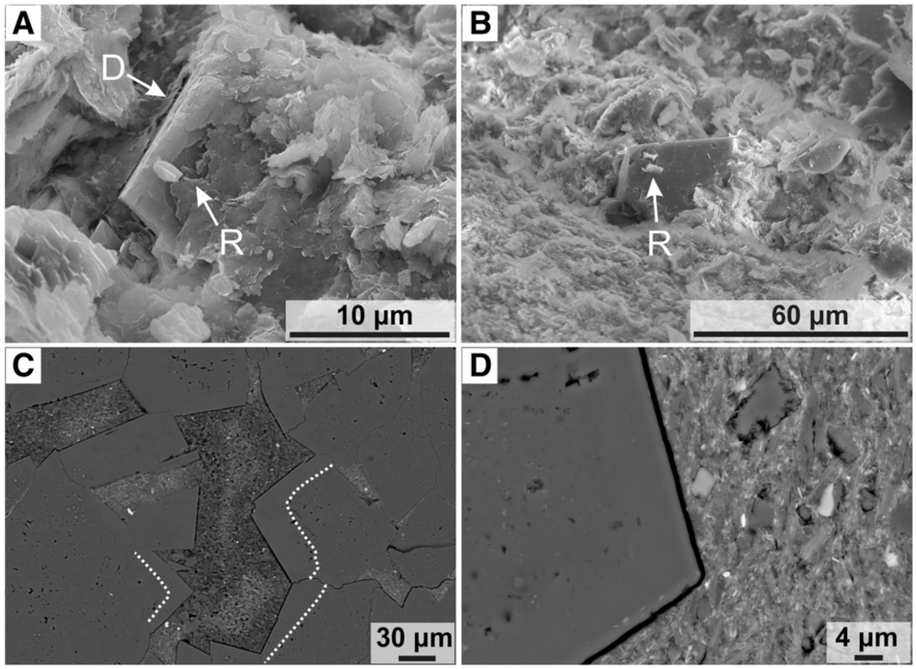

Fig. 10. SEM images of the different dolomite growth stages in a clayey matrix. A and B) First stage of replacive growth of dolomite crystal incorporating illitic clays (R of replacive). In A), a clear outer rim of dolomite crystal deforms clay minerals during the last growth stage (D of displacive). C and D) Later displacive growth resulting in clear outer rims (dotted lines) that deform muddy host ground mass.

hydrothermal processes (Lahcen et al., 2007). Calcite cement overlies previous authigenic minerals so postdate them. Calcite precipitation as well as dedolomitization processes are considered telodiagenetic products from flux of fresh oxidizing meteoric waters (Molenaar, 1998).

5.3. Diagenetic evolution and implications on reservoir quality

Amount and type of rip-up clasts occurring in fluvial Triassic deposits of the Argana Basin are a key first-order control over diagenetic history of host sandstones (Fig. 11). Its influence is particularly evident on mechanical compaction and dolomite cementation (Fig. 12). Both eodiagenetic processes are crucial for a thorough understanding of reservoir quality evolution.

On the one hand, mechanical compaction is strongly favored by muddy rip-up clast occurrence (Fig. 11A and B) behaving as highly ductile grains due to intragranular microporosity (Pittman and Larese, 1991) and lack of dolomite crystals. Their presence in sandstone framework results in a significant early reduction of primary porosity and an irreversible loss of IGV which considerably deteriorates reservoir quality (Rittenhouse, 1971; Pittman and Larese, 1991; Paxton et al., 2002; Worden and Morad, 2003; Figs. 11C; 12A). From Fig. 11B and C, it can be deduced that when around 20% of sandstone framework is represented by muddy rip-up clasts, COPL increases up to around 35% whereas IGV decreases to less than a 10% remaining. Effect of other relatively ductile framework components, such as lithic fragments (phyllite and schist), is subordinated to the abundance of this rip-up clast type as demonstrated by the greater correlation between muddy rip-up clasts and COPL (Fig. 11B and D). Conversely, dolomite crystalline rip-up clasts act as rigid (non-deformed) framework grains that prevent porosity loss by mechanical compaction (Figs. 5D to H; 12C). Ductility (grade of mechanical deformation) of dolomitic muddy rip-up clasts will depend on abundance and size of dolomite crystals within the clast (see difference in clast extrusion between Figs. 5B and C; 12B).

On the other hand, occurrence of dolomite crystalline and dolomitic muddy rip-up clasts has double role on eodiagenetic dolomite precipitation (Figs. 11E to H; 12B and C): 1) as nuclei for syntaxial dolomite cement to grow in adjacent interstitial space (Burley, 1984; Carvalho et al., 1995; Molenaar, 1998; Ketzer et al., 2002; Al-Ramadan et al., 2005; Fig. 9C); and 2) as local sources of dolomite cement derived from dissolution–reprecipitation processes (i.e. chemical compaction) (Arribas et al., 1996; Al-Ramadan et al., 2005; Morad et al., 2010; De Ros and Scherer, 2012). Petrographic evidences such as the greater correlation between this rip-up clast type and dolomite cement, compared with other cements (CEPL or total carbonate cement) (Fig. 11F to H), as well as similar chemical compositions of detrital dolomite and dolomite cements (Fig. 7A) are consistent with both processes. Fig. 11H suggests that when around 10% of sandstone framework is represented by these types of rip-up clasts (dolomite crystalline and dolomitic muddy), dolomite cement only can constitute up to 25% of total rock composition (including framework, cements and pores). Typical association of dolomite crystalline and dolomitic muddy rip-up clasts with coarser-grained depositional facies may also stimulate dolomite precipitation due to higher original permeability of such facies. Early pervasive dolomite cementation occludes remnant primary porosity but partially inhibits mechanical compaction, thus preserving high IGV in host sandstones. In the case of pre-compactional, fine-grained, rhombic dolomite cement from T7/T8 straight channel samples (Fig. 9D), primary porosity is also preserved. Despite the negative effect of dolomite cementation by reducing primary porosity, preservation of IGV may considerably enhance reservoir quality by later carbonate dissolution processes (Schmidt and McDonald, 1979; Surdam et al., 1984, Bjørlykke, 1984).

In addition, spatial distribution and abundance of different reported rip-up clasts are strongly facies-related according to grain size (Garzanti, 1991; Pittman and Larese, 1991). Preferential concentration of muddy rip-up clasts in continuous layers (Fig. 3B) and of dolomite crystalline rip-up clasts in specific depositional facies (e.g. channel-lags) increases porosity heterogeneity and permeability anisotropy. At pore- and depositional-scales, continuous levels of pseudomatrix blocking pore throats and intergranular pores (Fig. 12A; Bloch, 1994; Ketzer and Morad, 2006) as well as laterally extensive layers pervasively cemented by dolomite may constitute local barriers and baffles for fluid flow in-between amalgamated sandstone bodies, creating reservoir compartmentalization (Fig. 12B and C; Gibbons et al., 1993; Prosser et al., 1993).

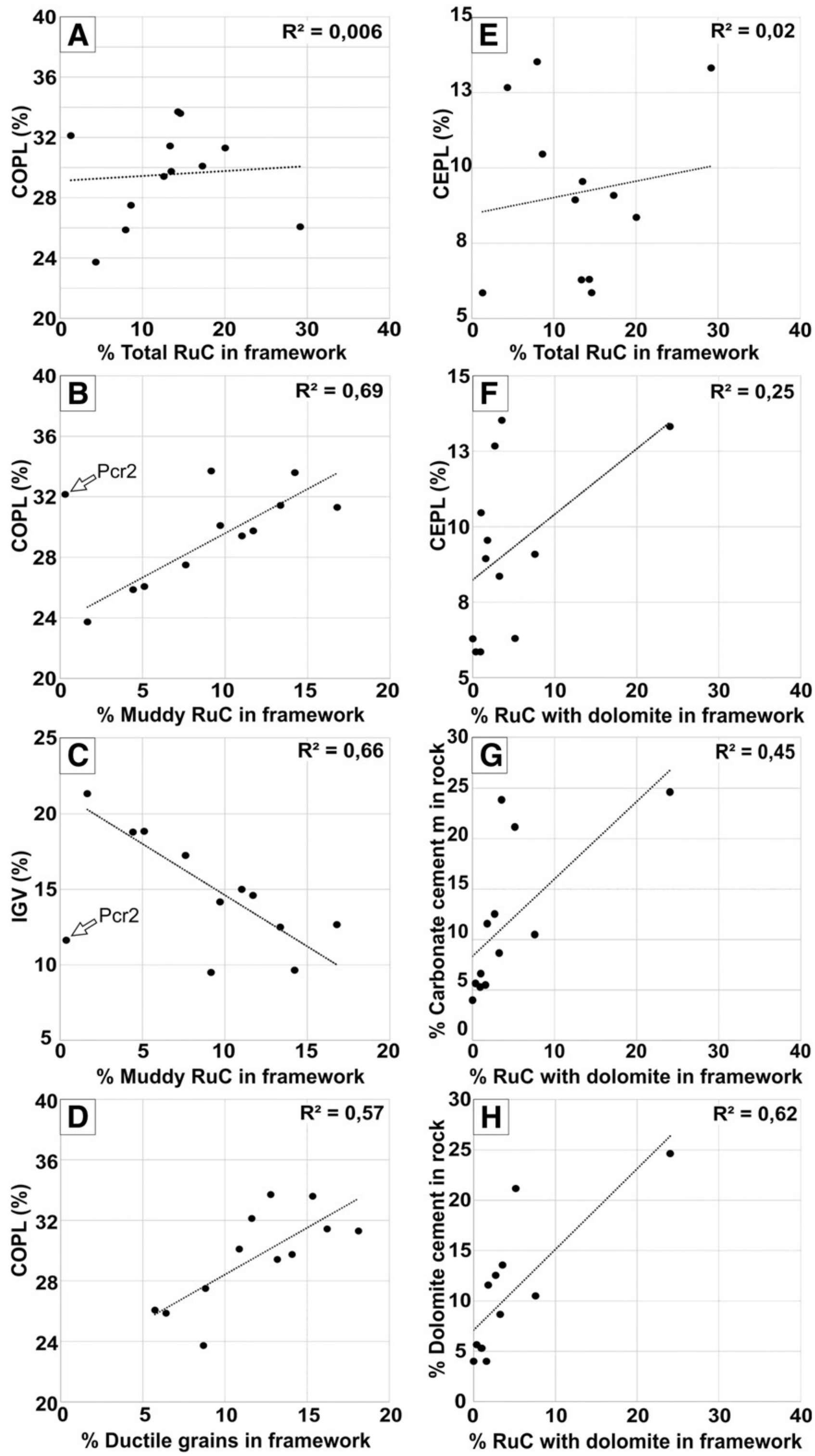

Fig. 11. Relationship between main diagenetic processes affecting host sandstones and the abundance of rip-up clast types. A) COPL versus percentage of all rip-up clast types in sandstone framework showing no apparent correlation according to its low R^2 value. B) COPL versus percentage of muddy rip-up clasts in sandstone framework showing very high and direct correlation as indicated by the highest R^2 value. PCr2 sample (T7/T8 straight channel) is not included for correlation because of significant predominance of lithic fragments over muddy rip-up clasts mainly influences mechanical compaction. C) IGV versus percentage of muddy rip-up clasts in sandstone framework shows high but inverse correlation. Idem with PCr2 sample. D) COPL versus percentage of ductile grains (muddy rip-up clasts plus lithic rock fragments) in sandstone framework shows high and direct correlation although slightly lower that only compared with muddy rip-up content. E) CEPL versus percentage of all rip-up clast types in sandstone framework shows no apparent correlation according to its very low R^2 value. F) CEPL versus percentage of rip-up clasts with dolomite (dolomitic muddy plus dolomite crystalline rip-up clasts) in sandstone framework shows low and direct correlation. G) Percentage of carbonate cements (dolomite plus calcite) in total rock composition versus percentage of rip-up clasts with dolomite in sandstone framework still shows relative low and direct correlation, although greater than previous one. H) Percentage of rip-up clasts with dolomite (dolomitic muddy plus dolomite crystalline rip-up clasts) in sandstone framework versus percentage of only dolomite cement in rock composition (framework, cement and pores) shows high and direct correlation according to its high R^2 value.

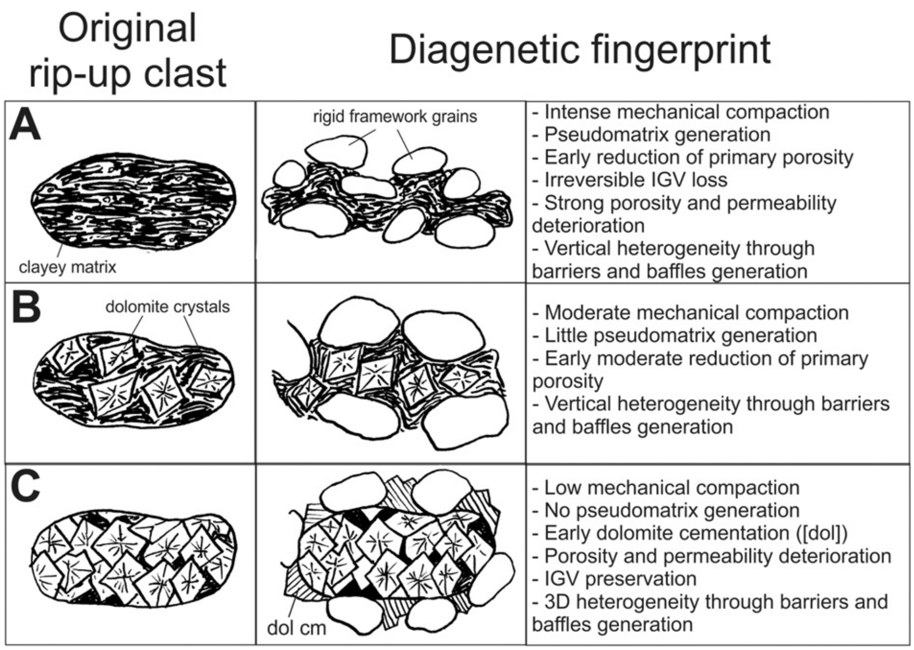

Fig. 12. Cartoon illustrating diagenetic behavior of the different rip-up clast types and related reservoir quality pathways. A) Muddy rip-up clasts. B) Dolomitic muddy rip-up clasts. C) Dolomite crystalline rip-up clasts.

6. Conclusions

Coupling high-resolution petrographic and chemical data within a well-constrained depositional framework of Triassic fluvial sandstones from Argana Basin (T6 and T7/T8 units), leads to following conclusions:

(1) Rip-up clasts may represent a significant part of host sandstone framework as intrabasinal components with a spatial distribution strongly controlled by depositional facies (i.e. grain size). Importance of muddy and dolomite rip-up clasts in fluvial sandstones is proved in two fundamental ways: 1) as information sources about low preservation potential floodplain deposits for paleogeographic reconstructions; and 2) as key elements controlling host sandstone diagenetic evolution and, thus, reservoir quality.
(2) On the basis of rip-up clast composition and mechanical behavior, three main classes are differentiated: muddy rip-up clasts without dolomite crystals; dolomitic muddy rip-up clasts with intermediate dolomite crystal proportions; and dolomite crystalline rip-up clasts mainly composed by dolomite crystals.
(3) Origin of these grains is related to erosion of coeval phreatic dolocretes, in different development stages, and associated muddy floodplain sediments in an evaporation-dominated environment. Cloudy cores with radial-pattern inclusions and clear outer rims in dolomite crystals suggest a first replacive and subsequent displacive crystal growth, respectively, in shallow environments.
(4) Diagenetic evolution, dominated by mechanical compaction and dolomite cementation, is strongly affected by the amount and type of rip-up clasts. Mechanical compaction of highly ductile muddy rip-up clasts results in early reduction of primary porosity and irreversible loss of IGV. High correlation ($R^2 = 0.69$) between COPL and this rip-up clast type indicates that when around 20% of sandstone framework is represented by muddy rip-up clasts, COPL increases up to around 35% whereas IGV decreases to less than a 10% remaining. Conversely, dolomite crystalline rip-up clasts act as rigid (non-deformed) framework grains preventing mechanical compaction. High correlation between dolomite cement and rip-clasts with dolomite crystals ($R^2 = 0.62$) points out that they may act as nuclei and source for dolomite cement, which can constitute up to 25% of total rock composition when these grains represent around 10% of sandstone framework. Their similar chemical compositions also support an early diagenetic origin coinciding with coeval phreatic dolocretes.
(5) Spatial distribution of rip-up clasts throughout depositional facies and associated diagenetic processes impact reservoir quality by generation of vertical and 3D fluid flow baffles and barriers that compartmentalize the reservoir.
(6) These results may be used for a better understanding of reservoir quality distribution in analogous hydrocarbon-bearing basins such as the Bay of Fundy, Nova Scotia (Canada).

Acknowledgments

Funding was provided by research projects CGL2013-43013-R (MINECO-FEDER), CGL2011-22709, CGL2014-52670-P and MAT02012-34473, as well as by the research group RNM369 and RNM179 (JA). Thanks to the Crimidesa Maroc company which provided logistical support during field work.

References

Allen, J.R.L., Wright, V.P., 1989. Paleosols in siliciclastic sequences. University of Readings. PRIS Short Course Notes Vol. 1.
Al-Ramadan, K., Morad, S., Proust, J.N., Al-Aasm, I.S., 2005. Distribution of diagenetic alterations in siliciclastic shoreface deposits within a sequence stratigraphic framework: evidence from the Upper Jurassic, Boulonnais, NW France. Journal of Sedimentary Research 75, 943–959.
Andrews, J.E., 1985. The sedimentary facies of a late Bathonian regressive episode: the Kilmaluag and Skudiburgh Formations of the Great Estuarine Group, Inner Hebrides, Scotland. Journal of the Geological Society (London) 142, 1115–1137.
Arakel, A.V., 1986. Evolution of calcrete in palaeodrainages of the Lake Narpperby area, Central Australia. Palaeogeography, Palaeoclimatology, Palaeoecology 54, 283–303.
Arakel, A.V., Jacobson, G., Salehi, M., Hill, C.M., 1989. Silicification of calcrete in palaeodrainage basins of the Australian arid zone. Australian Journal of Earth Sciences 36, 73–89.
Arakel, A.V., Jacobson, G., Lyons, W.B., 1990. Sediment–water interaction as a control on geochemical evolution of playa lake systems in the Australian arid interior. Hydrobiology 197, 1–12.

Arche, A., López-Gómez, J., 2014. The Carnian Pluvial Event in Western Europe: new data from Iberia and correlations with the Western Neotethys and Eastern North America–NW Africa regions. Earth Science Reviews 128, 196–231.
Armenteros, I., Bustillio, M.A., Blanco, J.A., 1995. Pedogenic and groundwater processes in a closed Miocene basin (northern Spain). Sedimentary Geology 99, 17–36.
Armenteros, I., Ben Brahim, M., Blanco, J.A., Huerta, P., Suárez, M., 2003. Costras carbonatadas en la sucesión aluvial distal eocena de la Formación Hamada de Boudenib II al sur del Alto Atlas (Marruecos). Geogaceta 34, 199–202.
Arribas, J., 1987. Origen y significado de los cementos en las areniscas de las facies Buntsandstein (Rama Aragonesa de la Cordillera Ibérica). Cuadernos de Geología Ibérica 11, 535–556.
Arribas, J., Díaz Molina, M., Tortosa, A., 1996. Ambientes de Sedimentación, procedencia y diagénesis de depósitos de ríos meandriformes desarrollados sobre playa-lakes. Mioceno de la Cuenca de Loranca (provincias de Cuenca y Guadalajara). Cuadernos de Geología Ibérica 21, 319–343.
Baudon, C., Redfern, J., Van Den Driessche, J., 2012. Permo-Triassic structural evolution of the Argana Valley, impact of the Atlantic rifting in the High Atlas, Morocco. Journal of African Earth Sciences 65, 91–104.
Bjørlykke, K., 1984. Formation of secondary porosity: how important is it? In: McDonald, D.A., Surnam, R.C. (Eds.), Clastic Diagenesis. AAPG Memoir Vol. 37, pp. 277–286
Bjørlykke, K., 1994. Fluid-flow processes and diagenesis in sedimentary basins. In: Parnell, J. (Ed.), Geofluids: Origin, Migration and Evolution of Fluids in Sedimentary Basins. Geological Society Special Publication Vol. 78, pp. 127–140.
Bloch, S., 1994. Effect of detrital mineral composition on reservoir quality. In: Wilson, M.D. (Ed.), Reservoir Quality Assessment and Prediction in Clastic Rocks. SEPM Short Course Vol. 30, pp. 161–182.
Bridge, J.S., Collier, R.E.Ll, Alexander, J., 1998. Large-scale structure of Calamus river deposits revealed using ground-penetrating radar. Sedimentology 45, 977–985.
Broughton, P., Trépanier, P., 1993. Hydrocarbon generation in the Essaouira basin of western Morocco. AAPG Bulletin 77, 999–1015.
Brown, R.H., 1980. Triassic rocks of the Argana Valley, southern Morocco, and their regional structural implications. AAPG Bulletin 64, 988–1003.
Burley, S.D., 1984. Patterns of diagenesis in the Sherwood Sandstone Group (Triassic), United Kingdom. Clay Minerals 19, 403–440.
Calder, J.H., Boehner, R.C., Brown, D.E., Gibling, M.R., Mukhoppadhyay, P.K., Ryan, R.J., Skilliter, D.M., 1998. Classic Carboniferous sections of the Minas and Cumberland Basins in Nova Scotia with special reference to organic deposits. Society for Organic Petrology Annual Meeting Field Trip, 29–30 July, 1998. Nova Scotia Natural Resources Open File Report ME 1998–5.
Carvalho, M.V.F., De Ros, L.F., Gomes, N.S., 1995. Carbonate cementation patterns and diagenetic reservoir facies in the Campos Basin Cretaceous turbidites, offshore eastern Brazil. Marine and Petroleum Geology 12, 741–758.
Chen, X.Y., McKenzie, N.J., Roach, I.C., 2002. Distribution in Australia: calcrete landscapes. In: Chen, X.Y., Lintern, M.J., Roach, I.C. (Eds.), Calcrete: Characteristics, Distribution and Use in Mineral Exploration. Cooperative Research Centre for Landscape Environments and Mineral Exploitation, Perth, Western Australia, pp. 110–138.
Colson, J., Cojan, I., 1996. Groundwater dolocretes in a lake-marginal environments: an alternative model for dolocrete formation in continental settings (Danian of the Provence Basin, France). Sedimentology 43, 175–188.
De Ros, L.F., Scherer, C.M.S., 2012. Stratigraphic controls on the distribution of diagenetic processes, quality and heterogeneity of fluvial–aeolian reservoirs from the Reconcavo Basin, Brazil. International Association of Sedimentologists. Special Publication 45, 105–132.
Di Giulio, A., Valloni, R., 1992. Analisi microscopica delle areniti terrigene: parametri petrologici e composizioni modali. Acta Naturalia di "L'Ateneo Parmese" 28, 55–101.
Dickinson, W.R., 1985. Provenance relations from detrital modes of sandstones. In: G.G. Zuffa (Ed.), Provenance of Arenites. NATO ASI Series C-148, 333–362.
Ellouz, N., Patriat, M., Gaulier, J.-M., Bouatmani, R., Sabounji, S., 2003. From rifting to Alpine inversion: Mesozoic and Cenozoic subsidence history of some Moroccan basins. Sedimentary Geology 156, 185–212.
El-Sayed, M.I., Fairchild, I.J., Spiro, B., 1991. Kuwaiti dolocretes: petrology, geochemistry, and groundwater origin. Sedimentary Geology 73, 59–75.
Fiechtner, L., Friedrichsen, H., Hammerschmidt, K., 1992. Geochemistry and geochronology of Early Mesozoic tholeiites from Central Morocco. International Journal of Earth Sciences 81, 45–62.
Garzanti, E., 1991. Non-carbonate intrabasinal grains in arenites: their recognition, significance, and relationship to eustatic cycles and tectonic setting. Journal of Sedimentary Petrology 61, 959–975.
Garzanti, E., Haas, R., Jadoul, F., Young, T.P., 1989. Irostones in the Mesozoic passive margin sequence of the Thetys Himalaya (Zanskar, Northen India: sedimentology and metamorphism. In: Taylor, W.E.G. (Ed.), Phanerozoic Ironstones. Geological Society of London, pp. 229–244.
Gibbons, K., Hellem, T., Kjemperud, A., Nio, S.D., Vebenstad, K., 1993. Sequence architecture, facies development and carbonate-cemented horizons in the Troll Field reservoir, offshore Norway. In: Ashton, M. (Ed.), Advances in Reservoir Geology. Geological Society of London Special Publication Vol. 69, pp. 1–31.
Gluyas, J., Cade, C.A., 1997. Prediction of porosity in compacted sands. In: Kupecz, J.A., Gluyas, J., Bloch, S. (Eds.), Reservoir Quality Prediction in Sandstones and Carbonates. AAPG Memoir Vol. 69, pp. 19–27.
Goudie, A.S., 1983. Calcrete. In: Goudie, A.G., Pye, K. (Eds.), Chemical Sediments and Geomorphology: Precipitates and Residua in the Near-Surface Environment. Academic Press, London, pp. 93–131.
Hardie, L.A., 1987. Perspectives on dolomitization: a critical view of some currents views. Journal of Sedimentary Petrology 57, 166–183.
Hay, W.W., Behensky Jr., J.F., Barron, E.J., Sloan, J.I., 1982. Late Triassic palaeoclimatology of the proto-central North Atlantic rift system. Palaeogeography, Palaeoclimatology, Palaeoecology 40, 13–30.
Hofmann, A., Tourani, A., Gaupp, R., 2000. Cyclicity of Triassic to Lower Jurassic continental red beds of the Argana Valley, Morocco: implications for palaeoclimate and basin evolution. Palaeogeography, Palaeoclimatology, Palaeoecology 161, 229–266.
Hutton, J.T., Dixon, J.C., 1981. The chemistry and mineralogy of some South Australian calcretes and associated soft carbonates and their dolomitization. Journal of the Geological Society of Australia 28, 71–79.
Ingersoll, R.V., Bullard, T.F., Ford, R.L., Grimm, J.P., Pickle, J.D., Sares, S.W., 1984. The effects of grain size on detrital modes: a test of the Gazzi–Dickinson point-counting method. Journal of Sedimentary Petrology 54, 103–116.
Jalil, N.E., Dutuit, J.-M., 1996. Permian captorhinid reptiles from the Argana formation, Morocco. Palaeontology 39, 907–918.
Kearsey, T., Twitchett, J.R., Newell, A.J., 2012. The origin and significance of pedogenic dolomite from the Upper Permian of the South Urals of Russia. Geological Magazine 149, 291–307.
Kent, D.V., Olsen, P.E., Witte, W.K., 1995. Late Triassic–Earliest Jurassic geomagnetic polarity sequence and paleolatitudes from drill cores in Newark rift basin, eastern North America. Journal of Geophysical Research 100, 14065–14998.
Kessler, J.L.P., Soreghan, G.S., Wacker, H.J., 2001. Equatorial aridity in western Pangea: Lower Permian loessite and dolomitic paleosols in northeastern New Mexico, USA. Journal of Sedimentary Research 71, 817–832.
Ketzer, J.M., Morad, S., 2006. Predictive distribution of shallow marine, low-porosity (pseudomatrix-rich) sandstones in a sequence stratigraphic framework–example from the Ferron sandstone, Upper Cretaceous, USA. Marine and Petroleum Geology 23, 29–36.
Ketzer, J.M., Morad, S., Evans, R., Al-Aasm, I., 2002. Distribution of diagenetic alterations in fluvial, deltaic, and shallow marine sandstones within a sequence stratigraphic framework: evidence from the Mullaghmore Formation (Carboniferous), NW Ireland. Journal of Sedimentary Research 72, 760–774.
Khadkikar, A.S., Merh, S.S., Malik, J.N., Chamyal, L.S., 1998. Calcretes in semi-arid alluvial systems: formative pathways and sinks. Sedimentary Geology 116, 251–260.
Khalaf, F.I., 1990. Occurrence of phreatic dolocrete within Tertiary clastic deposits of Kuwait, Arabian Gulf. Sedimentary Geology 68, 223–239.
Klein, H., Voigt, S., Saber, H., Schneider, J., Hminna, A., Fisher, J., Lagnaoui, A., Brosig, A., 2011. First occurrence of a Middle Triassic tetrapod ichnofauna from the Argana Basin (Western High Atlas, Morocco). Palaeogeography, Palaeoclimatology, Palaeoecology 307, 218–231.
Kraus, M.J., 1999. Paleosols in clastic sedimentary rocks: their geologic applications. Earth-Science Reviews 47, 41–70.
Kupecz, J.A., Land, L.S., 1994. Progressive recrystallization and stabilization of early-stage dolomite: Lower Ordovician Ellenberger Group, west Texas. International Association of Sedimentologists. Special Publication 21, 255–279.
Lahcen, D., Brahim, O., Fida, M., 2007. Facteurs de contrôle et signification génétique des assemblages minéralogiques argileux du Trias-Lias d'Argana (Haut Atlas Occidental, Maroc). Comunicações Geológicas 94, 145–159.
Laville, E., Petit, J.-P., 1984. Role of synsedimentary strike-slip faults in the formation of Moroccan Triassic basins. Geology 12, 424–427.
Laville, E., Pique, A., 1991. La distension crustale atlantique et atlasique au Maroc au début du Mésozoïque: le rejeu des structures hercyniennes. Bulletin de la Societe Géologique de France 162 (6), 1161–1171.
Leikine, M., Medina, F., Ahmamou, M., 1996. Lack of low-grade metamorphism in the Triassic formations of the Argana Basin, Morocco: an illite crystallinity reevaluation. Journal of African Earth Sciences 22, 565–573.
Letourneau, P.M., Olsen, P.E., 2003. The Great Rift Valleys of Pangea in Eastern North America. Volume One: Tectonics, Structure and Volcanism. Columbia University Press (214 pp.).
Lundegard, P.D., 1992. Sandstone porosity loss. A 'big picture' view of the importance of Compaction. Journal of Sedimentary Petrology 62, 250–260.
Lunt, I.A., Bridge, J.S., Tye, R.S., 2004. Development of a 3-D depositional model of braided river gravels and sands to improve aquifer characterization. In: Bridge, J.S., Hyndman, D. (Eds.), Aquifer Characterization. SEMP Special Publication Vol. 80, pp. 139–169.
Mader, D., 1986. Braidplain, floodplain and playa-lake, alluvial fan, aeolian and palaeosol facies composing a diversified lithogenetical sequence in the Permian and Triassic of south Devon (England). In: Mader, D. (Ed.), Aspects of Fluvial Sedimentation in the Lower Triassic Buntsandstein of EuropeLecture Notes in Earth Sciences vol. 4. Springer, Berlin, pp. 15–64.
Mader, N.K., Redfern, J., 2011. A sedimentological model for the continental Upper Triassic Tadrart Ouadou Sandstone Member: recording an interplay of climate and tectonics (Argana Valley, South-west Morocco). Sedimentology 58, 1247–1282.
McKie, T., Aggett, J., Hogg, A.J., 1998. Reservoir architecture of the Upper Sherwood Sandstone Wytch Farm. In: Underhill, J.R. (Ed.), Development. Evolution and Petroleum Geology of the Wessex Basin. Geological Society Special Publication Vol. 133, pp. 399–406.
Medina, F., 1988. Tilted-blocks pattern, paleostress orientation and amount of extension, related to Triassic early rifting of the central Atlantic in the Amzri area (Argana Basin, Morocco). Tectonophysics 148, 229–233.
Medina, F., 1991. Superimposed extensional tectonics in the Argana Triassic formations (Morocco), related to the early rifting of the central Atlantic. Geological Magazine 128, 525–536.
Medina, F., 1995. Syn- and postrift evolution of the El Jadida–Agadir basin (Morocco): constraints for the rifting models of the central Atlantic. Canadian Journal of Earth Sciences 32, 1273–1291.
Miall, A.D., 2006. The geology of fluvial deposits. Sedimentary Facies, Basin Analysis, and Petroleum Geology. Springer-Verlag, Berlin Heidelberg (585 pp.).
Milnes, A.R., 1992. Calcrete. In: Martine, I.P., Chesworth, W. (Eds.), Weathering, Soils and Paleosols, Development in Earth Surface Processes 2. Elsevier, Amsterdam, pp. 309–347.

Molenaar, N., 1998. Origin of low-permeability calcite-cemented lenses in shallow marine sandstones and $CaCO_3$ cementation mechanisms: an example from the Lower Jurassic Luxemburg Sandstone, Luxemburg. In: Morad, S. (Ed.), Carbonate Cementation in Sandstones. International Association of Sedimentologists Special Publication Vol. 26, pp. 193–211.
Morad, S., Marfil, R., De la Peña, J.A., 1989. Diagenetic K-feldspar pseudomorphs in the Triassic Buntsandstein sandstones of the Iberian Range, Spain. Sedimentology 36, 635–650.
Morad, S., Al-Ramadan, K., Ketzer, J.M., De Ros, L.F., 2010. The impact of diagenesis on the heterogeneity of sandstone reservoirs: a review of the role of depositional facies and sequence stratigraphy. AAPG Bulletin 94, 1267–1309.
Mousavi, M.A., Bryant, S.L., 2013. Geometric models of porosity reduction by ductile grain compaction and cementation. AAPG Bulletin 97, 2129–2148.
Nash, D.J., McLaren, S.J., 2003. Kalahari valley calcretes: their nature, origins and environmental significance. Quaternary International 111, 3–22.
Odin, G.S., 1985. Significance of green particles (glaucony, berthierine, chlorite) in arenites. In: Zuffa, G.G. (Ed.)Provenance of Arenites Vol. 148. D. Reidel, NATO Advanced Study Institute, Dordrecht, Netherlands, pp. 279–307.
Olsen, P.E., 1997. Stratigraphic record of the Early Mesozoic breakup of Pangea in the Laurasia–Gondwana rift system. Annual Review of Earth and Planetary Sciences 25, 337–401.
Olsen, P.E., Kent, D.V., Fowell, S.J., Schlische, R.W., Withjack, M.O., LeTourneau, P.M., 2000. Implications of a comparison of the stratigraphy and depositional environments of the Argana (Morocco) and Fundy (Nova Scotia, Canada) Permian–Jurassic basins. In: Oujidi, M., Et-Touhami, M. (Eds.), Le Permien et le Trias du Maroc. Acte de la Premiere Reunion du Groupe Marocain de Permien et du Trias, Oujda, pp. 165–183.
Paxton, S.T., Szabo, J.O., Ajdukiewicz, J.M., Klimentidis, R.E., 2002. Construction of an intergranular volume compaction curve for evaluating and predicting compaction and porosity loss in rigid-grain sandstone reservoirs. AAPG Bulletin 86, 2047–2067.
Pettijohn, F.J., Potter, P.E., Siever, R., 1973. Sand and Sandstones. Springer-Verlag, Berlin (617 pp.).
Pimentel, N.L., Wright, V.P., Azevedo, T.M., 1996. Distinguishing early groundwater alteration effects from pedogenesis in ancient alluvial basins: examples from the Palaeogene of Portugal. Sedimentary Geology 105, 1–10.
Pittman, E.D., Larese, R.E., 1991. Compaction of lithic sands: experimental results and applications. AAPG Bulletin 75, 1279–1299.
Prosser, D.J., Daws, J.A., Fallick, A.E., Williams, B.P.J., 1993. Geochemistry and diagenesis of stratabound calcite cement layers within the Rannoch Formation of the Brent Group, Murchison Field, North Viking Graben (northern North Sea). Sedimentary Geology 87, 139–164.
Purvis, K., Wright, V.P., 1991. Calcretes related to phreatophytic vegetation from the Middle Triassic Otter Sandstone of South West England. Sedimentology 38, 539–551.
Rittenhouse, G., 1971. Mechanical compaction of sands containing different percentages of ductile grains: a theoretical approach. AAPG Bulletin 55, 92–96.
Schmidt, V., McDonald, D.A., 1979. The role of secondary porosity in the course of sandstone diagenesis. SEPM Special Publication 26, 209–225.gib.
Schmid, S., Worden, R.H., Fisher, Q.J., 2004. Diagenesis and reservoir quality of the Sherwood Sandstone (Triassic), Corrib Field, Slyne Basin, west of Ireland. Marine and Petroleum Geology 21, 299–315.
Schmid, S., Worden, R.H., Fisher, Q.J., 2006. Sedimentary facies and the context of dolocrete in the Lower Triassic Sherwood Sandstone Group: Corrib Field west of Ireland. Sedimentary Geology 187, 205–227.
Smoot, J.P., Castens-Seidell, B., 1994. Sedimentary features produced by efflorescent salt crusts, Saline Valley and Death Valley, California: sedimentology and geochemistry of modern and ancient Saline Lakes. In: Renaut, R.W., Last, W.M. (Eds.), Sedimentology and Geochemistry of Modern and Ancient Saline Lakes. SEPM Special Publications Vol. 50, pp. 73–90.
Spötl, C., Wright, V.P., 1992. Groundwater dolocretes form the Upper Triassic of the Paris Basin, France: a case study of an arid, continental diagenetic facies. Sedimentology 39, 1119–1136.
Surdam, R.C., Boese, S.W., Crossey, L.J., 1984. The chemistry of secondary porosity. In: McDonald, D.A., Surnam, R.C. (Eds.), Clastic Diagenesis. AAPG Memoir Vol. 37, pp. 127–149.
Tixeront, M., 1973. Lithostratigraphie et minéralisations cuprifères et uranifères stratiformes syngénétiques et familières des formations détritiques permo-triasiques du couloir d'Argana (Haut-Atlas occidental, Maroc). Notes du Service Géologique du Maroc 33, 147–177.
Viseras, C., Fernández, J., 2010. Sistemas aluviales de alta sinousidad. In: Arche, A. (Ed.), Sedimentología: del proceso físico a la cuenca sedimentaria. CSIC, Madrid, pp. 261–298.
Viseras, C., Fernández, J., Henares, S., Cuéllar, N., 2011. Facies architecture in outcrop analogues for the TAGI reservoir. Exploratory interest. AAPG Search and Discovery Article, AAPG International Conference and Exhibition, Milan, Italy, #90135.
Waugh, B., 1978. Authigenic K-feldspar in British Permo-Triassic sandstones. Journal of the Geological Society 135, 51–56.
Worden, R.H., Morad, S., 2003. Clay minerals in sandstones: controls on formation, distribution and evolution. In: Worden, R.H., Morad, S. (Eds.), Clay Mineral Cement in Sandstones. International Association of Sedimentologists Special Publication Vol. 34, pp. 3–41.
Wright, V.P., 1994. Losses and gains in weathering profiles and duripans. In: Parker, A., Sellwood, B.W. (Eds.), Quantitative Diagenesis: Recent Developments and Applications to Reservoir Geology. NATO ASI Series, Series C: Mathematical and physical sciences Vol. 453, pp. 95–123.
Wright, V.P., Tucker, M.E., 1991. Calcretes: an introduction. In: Wright, V.P., Tucker, M.E. (Eds.), CalcretesIAS Reprint Series vol. 2. Blackwell Scientific Publications, Oxford, pp. 1–22.
Zuffa, G.G., 1980. Hybrid arenites: their composition and classification. Journal of Sedimentary Petrology 50, 21–29.
Zuffa, G.G., 1985. Optical analyses of arenites: influence of methodology on compositional results. In: Zuffa, G.G. (Ed.), Provenance of Arenites, 148. D. Reidel, NATO Advanced Study Institute, Dordrecht, Netherlands, pp. 165–189.
Zuffa, G.G., 1987. Unravelling hinterland and offshore palaeogeography from deep-water arenites. In: Leggett, J.K., Zuffa, G.G. (Eds.), Marine Clastic Sedimentology: Concepts and Case Studies. Graham & Trotman, California, pp. 39–61.